JBIS
Journal of the British Interplanetary Society

VOLUME 78 NO.12 DECEMBER 2025

Special Issue:
Project Icarus: the final papers-4

www.bis-space.com

ISSN 0007-084X PUBLICATION DATE: 1 DECEMBER 2025

Submitting papers to JBIS

JBIS welcomes the submission of technical papers and letters for publication dealing with technical reviews, research, technology and engineering in astronautics and related fields.

Text should be:

- As concise as the content allows – typically 5,000 to 6,000 words. Shorter papers (Technical Notes) will also be considered; longer papers will only be considered in exceptional circumstances – for example, in the case of a major subject review.
- Source references should be inserted in the text in square brackets – [1] – and then listed at the end of the paper.
- Illustration references should be cited in numerical order in the text; those not cited in the text risk omission.
- Captions must be labelled with their Fig. number and should be as short as possible.

Illustrations should be:

- Colour or mono, but should be as close to print resolution (300 dpi) as possible. Poor-quality illustrations may compromise the acceptance of papers for publication. Images embedded in Word documents may be acceptable, but JBIS reserves the right to request separate higher-resolution image files from the author prior to publication.
- Responsibility for copyright clearance of images rests entirely with the author.

Submission of papers

- Papers for consideration should be sent by email to **jbis@bis-space.com** as **both** a Word document and as a Word PDF file (in order to check for font anomalies), together with any separate image files.
- If a paper is accepted for publication, the author will be asked to sign a License to Publish form. This can be downloaded at https://www.bis-space.com/write-for-us/jbis-submission-guidance/licence-to-publish/
- Authors will receive a complimentary copy of the issue in which their paper appears.

We respectfully ask authors to adhere to these guidelines. Failure to do so will result in the delay of acceptable papers for publication.

Our full Guidelines for Authors can be downloaded from **https://www.bis-space.com/write-for-us/jbis-submission-guidance/**

Past papers

- Past papers are available in PDF format at a cost of £5.00 per paper from **https://bis-space.com/shop/product-category/magazines/journal-of-the-bis/papers/**

International Advisory Board

Editor David Salt **Deputy Editor** Mark Hempsell **Associate Editors** Keith Cooper, Stephen Gamble, Paul Gilster, Rob Swinney, Griffith Ingram **Chief Administrator** Ted Davis **Production** MP3 Media **JBIS Office** British Interplanetary Society, Arthur C. Clarke House, 27-29 South Lambeth Road, London, SW8 1SZ, United Kingdom **tel** +44 (0)20 7735 3160
Subscriptions email subscriptions@bis-space.com
www.bis-space.com

DISTRIBUTION
JBIS is distributed worldwide by mail and may be received by annual subscription or purchase of single copies. It is available through membership of the British Interplanetary Society at much reduced rates. Subscription details for members, non-members and libraries are available from the above address.

JBIS is a publication that promotes the mission of the British Interplanetary Society. Opinions expressed in signed articles are those of the contributors and do not necessarily reflect the views of the Editor or the Council of the British Interplanetary Society. Security clearance, where necessary, is the responsibility of the author.

Published by the British Interplanetary Society. Registered Company No: 402498. Registered Charity No: 250556.
Printed in England by Buxton Press Ltd, Palace Road, Buxton, Derbyshire SK17 6AE

JBIS CONTENTS

VOLUME 78 NO.12 DECEMBER 2025

OUR MISSION STATEMENT

The British Interplanetary Society promotes the exploration and use of space for the benefit of humanity, connecting people to create, educate and inspire, and advance knowledge in all aspects of astronautics.

Project Icarus: The Pegasus Spacecraft Concept Design ICF Propulsion for an Interstellar Rendezvous Mission – Part A

K. F. LONG Interstellar Research Centre, Stellar Engines Ltd, 65 Peach Street, Wokingham, RG40 IXP, United Kingdom

Email interstellarresearchcentre@gmail.com

DOI https://doi.org/10.59332/jbis-078-12-0402

In the 1970s members of the British Interplanetary Society designed a spacecraft for an interstellar flyby mission to the nearest stars called Project Daedalus. In 2009 this author initiated a successor study called Project Icarus which set out to re-design the Daedalus spacecraft based on advances in science and technology. In this paper we describe a concept called Pegasus which is proposed as one of the potential improved solutions to the Daedalus. This is an inertial confinement fusion propelled spacecraft driven by laser beams, the technology for which is now supported by successful experiments at the National Ignition Facility. The Pegasus is a concept for an interstellar rendezvous mission carrying a 150 tonnes payload to 4.3 *ly* in a trip duration of order a century. It would be characterised by a thrust of 0.64 MN, a jet power of 2.85 TW and a specific power of 1.12 MW/kg. In this paper we discuss various physics and engineering issues relevant to the propulsion system. This paper is a final contribution to Project Icarus.

Keywords: Interstellar Studies, Fusion Propulsion, Pegasus, Project Icarus

1 INTRODUCTION

Project Icarus is a theoretical design study first initiated in 2009 which set out to design an interstellar probe [1, 2, 3]. A brief history of the origin of the project has previously been described [4]. It was to be based on the British Interplanetary Society Project Daedalus study [5], an interstellar flyby probe carrying a 450 tonnes payload to be sent to Barnard's star 5.9 *ly* away in a total trip time of order half a century (originally it was defined as a 40 year mission), based on evidence at the time for a planetary companion [6]. In contrast, Project Icarus sets out to design an interstellar rendezvous probe carrying 150 tonnes payload mass to 4.3 *ly* in a trip time of order one century.

The decision to extend the Project Icarus mission to a century was made to ease the engineering requirements of the system, especially considering the use of deceleration and this decision is consistent with research by others which suggested more time would be needed [7]. The mission for Project Icarus was also changed to a new astronomical target, which is any exoplanets around the Centauri A/B system. The vehicles in Project Daedalus and Project Icarus are types of nuclear pulse propulsion systems, and an excellent review is given by Martin and Bond [8] who also conducted a post-review of the Daedalus design worth reading [9].

An achievement of the project has been the development of several vehicle concepts [10] and the results of this work have been written up in a separate paper [11]. One of the most prominent of these is the z-pinch driven Firefly, which has been published in the literature [12, 13, 14], although other concepts have also been developed along the way including a plasma jet magneto inertial fusion propulsion system [15] and an Ultra-dense Deuterium concept [16]. A good review of this work has been presented by others [10]. All these concepts have in common the use of a fusion advanced propulsion engine [17] which aims to achieve thermonuclear ignition of hydrogen isotopes based on the Lawson criteria [18]. The US space agency NASA has a long-standing interest in the potential of spacecraft driven by fusion reactions [19], and it is also an active field of research in academia [20].

The Daedalus was an inertial confinement fusion (ICF) propulsion engine but driven by electron beams [21, 22]. For the work discussed in this paper the design is ICF based but driven by lasers as the principal means of energy deposition to the fuel. This is particularly important since recently thermonuclear ignition within a laboratory experiment has been demonstrated at the National Ignition Facility (NIF) for an energy input of E_{in} = 2.05 MJ and energy output of E_{out} = 3.15 MJ was achieved which corresponds to a gain of G = 1.5 [23, 24, 25, 26], so this is a critical point of experimental validation for the propulsion system. Thermonuclear fusion via the ICF method has also been validated historically through the Halite-Centurion programme which is partly described elsewhere [27]. The physics of ICF is highly complex and requires numerical modelling tools to give some understanding of the operation and performance of any implosion engine. That said, there are reliable texts available to guide simple first estimates [28, 29]. Indeed, such an approach was used in the design of the Pegasus, and it involved a Representative Physics Model which is described in a separate paper written in parallel with this one [30].

In previous work this author has discussed the development of concept design models to meet the requirements for Project Icarus including a description of *Leviathan* [31], *Resolution*, *Endeavour* and Pegasus Mk1 [32]. In particular, the design approach and methodology were described which ultimately led to the final solution as a process of down select. These models were designed in a Fortran 95 code written by this author called HeliosX which has been described elsewhere [33, 34, 35, 36] and has also been applied to an interstellar precursor mission called *SunVoyager* [37, 38] and a crewed gas giant mission called *Discovery-III* [39]. Where possible, HeliosX (and the design of Pegasus) were mostly written in response to recommendations from NASA and a need to develop consistent modelling methods for fusion propulsion [40, 41].

In this paper, we now present a revised and final model for the Pegasus to include more detailed calculations, and we refer to this as Pegasus *Mk2*. In a separate paper we have given a description for the other engineering systems associated with the Pegasus spacecraft [42], to include the structural configuration, science payload, mission profile and other systems associated with the design. This is also supported by independent papers written by others which help to define these other engineering systems and some of the assumptions to be adopted in the design work [43, 44, 45]. We have also given a detailed description of the propulsion power cycle [46].

In this paper the emphasis will be on the propulsion system. It will be clear that some of the system definitions have not been completed, and this was mainly due to time, in a project that had continued for many years, so this represents the design at the time of this close out. It is fully acknowledged that a lot more work could have been completed to further improve the definition of the spacecraft had the project continued.

1 CONFIGURATION & PERFORMANCE

In a conventional rocket engine, the exhaust velocity is directly related to the temperature inside the reaction chamber, where the temperature of the expanding gas is a measure of how fast the molecules are moving. In the vacuum of space, it is given as a function of the temperature of the combustion chamber T, ratio for specific heats of the exhaust gas γ, molar mass of exhaust gas M and the universal gas constant R such that:

$$v_{ex} = \sqrt{\frac{2\gamma RT}{(\gamma-1)M}} \tag{1}$$

Where the higher the combustion chamber temperature, and the lower the molecular weight, the higher the exhaust velocity. We might refer to this as a thermal rocket, where any combusted products are heated to an equilibrium temperature with other materials and then expand through the nozzle. However, in a fusion engine, unless the fusion products are first used to heat a propellant, then the exhaust velocity is not a function of the temperature but the energy of individual particles of mass m as follows:

$$v_{ex} = \sqrt{\frac{2E}{m}} \tag{2}$$

The reason the exhaust velocity is not a function of the temperature is because the charged particle products from the reactions will not contact the reaction chamber wall. Instead, they are directed using a magnetic nozzle for thrust generation. As a result, a fusion engine has the potential for a much higher exhaust velocity than a thermal rocket. Note also that Equation (2) is for non-relativistic flight and to account for relativistic flight we would be required to use relationships from special relativity, but that will not be necessary for the low speeds studied in this work. However, the performance of the fusion engine is dependent on temperature in a different way, which is the temperature required for the charged particles of density n to overcome the Coulomb barrier and react under confinement time τ, the product of which is referred to as the Lawson Criterion $nT\tau \geq$ constant [18].

For Project Icarus the defined distance is 4.3 *ly* and the defined trip time is around 100 years. This implies a velocity increment of around ~12,900 km/s to complete the mission, neglecting time for acceleration and deceleration. Even if we adopted the optimum mass ratio of $R = 4.9$ as defined by Shepherd [47] this implies a minimum exhaust velocity exceeding ~8,100 km/s, or an equivalent specific impulse close to ~10^6 s, which is the sort of level required for interstellar missions [48]. A similar minimum specific impulse was determined for an interstellar mission lasting decades in duration from considerations of an energy limited minimum flight time mission [49]. This is therefore one of the reasons why fusion is a preferred fuel choice since it can offer this performance.

For the Pegasus, we will adopt a D^3He fuel. This is because the fuel combinations of DD and DT lead to the production of substantial neutrons which then suggests a need for large shielding mass. Whilst the D^3He reaction will also lead to neutron production, via DD self-burn secondary reactions (and DT Tertiary), it is largely aneutronic. The charged particle productions from the reaction, protons and ^4He, can also be directed magnetically for thrust, although we acknowledge that the reaction is more difficult to ignite than DD or DT and requires a higher temperature. For a D^3He fuel (with mass defect α = 0.0039), as adopted in this work, with a specific energy of order 3.5×10^{11} J/g, this computes to a maximum theoretical exhaust velocity given by substitution of the energy $E = \alpha mc^2$, (where α is the mass defect) into Equation (2) as follows:

$$v_{ex} \approx (2\alpha)^{1/2}c = 26{,}500\ km/s \tag{3}$$

However, considering a burn-up fraction (the amount of fuel burned through fusion reactions and converted into usable charged particles for thrust) like the value adopted for the Daedalus study of $\phi = 13.3 \rightarrow 17.5\%$, this significantly reduces the potential exhaust velocity to:

$$v_{ex} \approx (2\alpha\phi)^{\frac{1}{2}}c = 9{,}650 \rightarrow 11{,}076\ km/s \tag{4}$$

Yet, then we must factor in the divergence of the exhaust jet which is related to the energy losses from the system. For the Daedalus engine this was near perfect at around $\mu_j = 91\%$ and so taking this into account we can see how the exhaust velocity is reduced further still which brings us approximately to the two exhaust velocities adopted for the Daedalus study:

$$v_{ex} \approx \left(2\alpha\phi\mu_j\right)^{\frac{1}{2}}c = 9{,}210 \rightarrow 10{,}600\ km/s \tag{5}$$

Therefore, in deriving a new design, if the burn-up fraction or jet efficiency are higher, towards a more ideal rocket, we can expect a higher exhaust velocity. Similarly, if the burn-up fraction or jet efficiency are lower, then this indicates there are more energy losses from the system and so we should expect a lower exhaust velocity. If the exhaust velocity is lower for the same velocity increment, we must aim for a design that has a higher mass ratio to give an equivalent performance, which means a leaner propellant design.

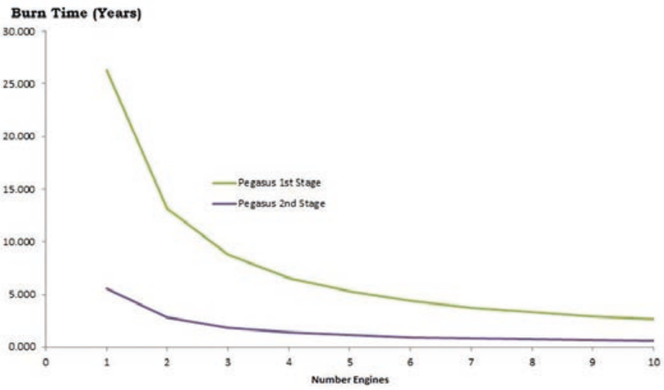

Fig.1 Calculations for Pegasus Burn Time with Number of Engines.

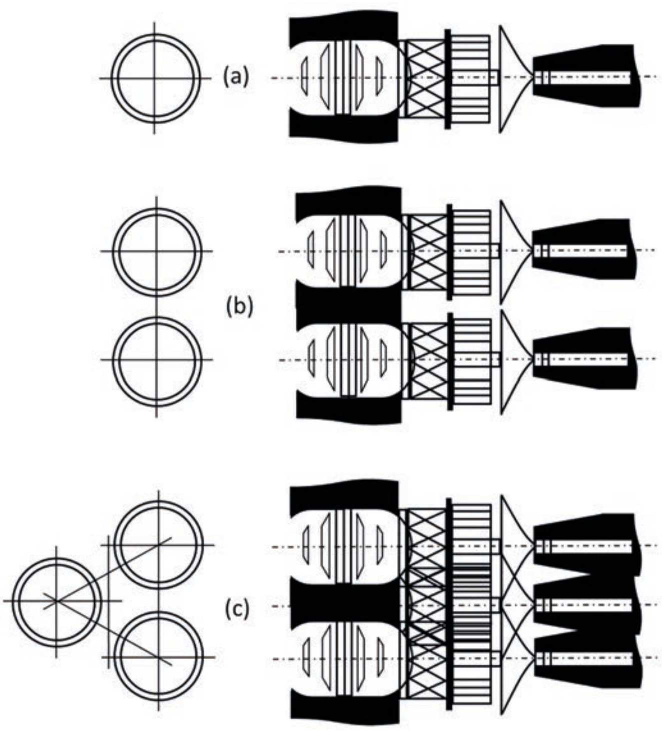

Fig.2 Propulsion Configurations (a) 1-engine (b) 2-engines (c) 3-engines.

It has been shown that parallel staging offers an advantage over a series staging design when the exhaust velocity approaches the optimum value [49]. In earlier work we studied a 5-engine vehicle configuration called *Endeavour* for a parallel thrust profile [32]. However, it was necessary to perform a re-evaluation of the *Endeavour* spacecraft concept since it was realized that there was a major failure mode that had been neglected. In particular, the 5 engines were near to each other so that when the ICF capsules were detonated at high repetition rate they would release significant amounts of Bremsstrahlung x-ray and high MeV neutron radiation. This radiation would be absorbed into the engine bell material and the surrounding structure leading to a weakening of its material strength. It was realised therefore that radiation shields need to be constructed around the engine bells to separate them from each other.

Fig. 1 shows the effect on the acceleration stage (1st stage) and deceleration stage (2nd stage) burn time with increasing number of engines for the Pegasus multi-engine configuration based on calculations conducted early on for the Mk1 design. It is observed that increasing the number of engines does minimise the burn time but at the cost of increased propulsion mass. Figs 2-4 show the different sorts of reaction chamber configurations considered for both *Endeavour* and Pegasus to include from a single engine (which is equivalent to *Resolution* [32]) all the way up to a 7-engine arrangement.

However, fitting the radiation shields was not easy unless one removed the central engine. For this reason, the design evolved to a 4-engine staged parallel thrust design, with the radiation shields intersecting towards the centre of the engine arrangement and this is called Pegasus, a ship named after the mythical winged divine horse from Greek mythology (Pegasus was ridden by Bellerophon as he slayed the Chimera). The Pegasus then became one of the proposed alternative design solutions to the historical Daedalus design, the purpose for which Project Icarus was initiated.

Fig. 5 shows the parallel thrust engines cutaway, and how it is envisaged that the laser systems would be connected to the reaction chambers. Figs 6 and 7 illustrate the Pegasus concept design with its 4-engine configuration arrangement. They illustrate a rear view showing the engine reaction chambers as a cut-away as well as a front view showing the positioning of the propellant tanks. Also shown in the illustrations are the large

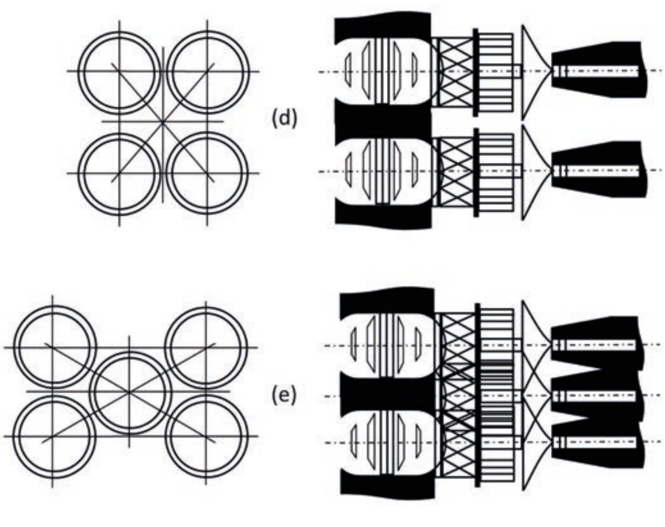

Fig.3 Propulsion Configurations (d) 4-engines (e) 5-engines.

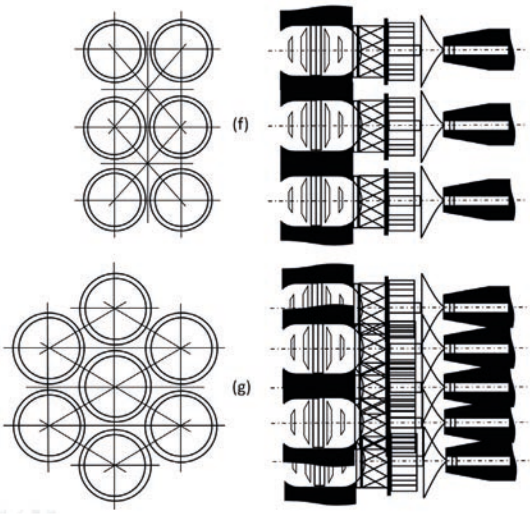

Fig.4 Propulsion Configurations (f) 6-engines (g) 7-engines.

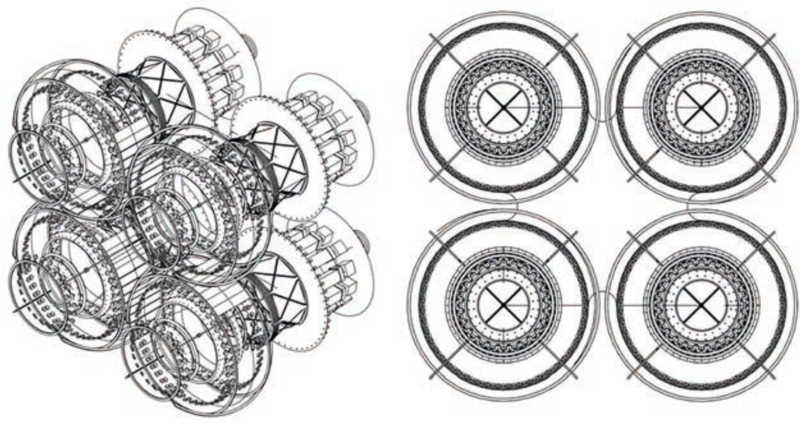

Fig.5 Pegasus Parallel Thrust Four-Engine Configuration.

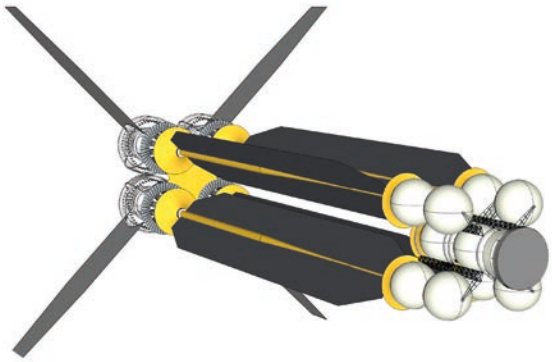

Fig.6 Spacecraft Pegasus Concept Design Frontal View.

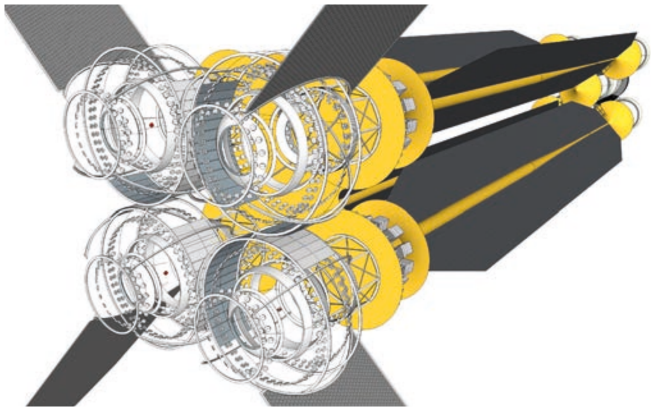

Fig.7 Spacecraft Pegasus Concept Design Rear View.

thermal radiators for dumping excess heat. This will mainly be generated from the laser drivers but also from the fusion engines and this is why there are two different sets to account for separate heat emission rates. We assumed 900 K associated with the laser driver and induction system, and 2,500 K associated with the engines.

Another major change to appear in the Pegasus design would be the design of the ICF pellet. Although Pegasus was to adopt a similar (but smaller) capsule design to the Daedalus second stage engine, it was thought prudent to tailor for a larger ablator shell size (outer layer of capsule) and a larger density of Helium-3 towards the outer edge of the fuel, to help mitigate the radiation release. The description of the preferred capsule specification is more a statement of preference in terms of how pellet designs can be optimised towards the application of space propulsion. Although the pellet was designed [30] in such a way to maintain burn-up fraction consistency with the Daedalus second stage at $\phi = 0.133$ so that the exhaust velocity could also be maintained (initially at 9,210 km/s but was later reduced to 8,897 km/s). Therefore, apart from a largely aneutronic fuel choice in D^3He, Pegasus would mitigate the radiation release by five ways to protect the spacecraft and reduce the probability of mission failure:

1. High energy 2.45 MeV and 14 MeV neutrons released from secondary DD self-burn and tertiary DT respectively [50] are mostly captured into a higher density Helium-3 fuel layer where the capture reaction probability is increased.
2. Any emitted x-rays that escape from the thermonuclear burn within the fuel are absorbed into the thick ablator shell made up of a strong absorber material.
3. Any further x-rays or neutrons that escape is then absorbed into an insulation layer internal to the thrust chamber wall.
4. Inclusion of radiation shields at the location of critical technology systems for final thermalization of neutrons, where the thermalization rate decreases linearly across the thickness of the shield so that it is zero at the other side.
5. External shields are included around the thrust chamber and in between them to protect them from each other and to protect the surrounding spacecraft structure.

In an earlier paper by this author a preliminary mission profile and performance was shown for the Pegasus spacecraft Mk1 design [32]. Since the publication of that work further work has now been done to refine the design concept with calculations at a higher level of fidelity [42] in which a mission to the nearest stars is demonstrated in a timescale of order one century. This is the Pegasus Mk2 design.

Table 1 shows a mass budget for the Pegasus spacecraft propulsion system, in addition to the power supply (which is contained within the payload). The 150 tonnes payload mass was the main mission requirement, and the other numbers fall from this value. Starting with the propellant mass, then the structural mass to hold that propellant and then the various power and propulsion associated technologies to enable that engine to give the desired performance so that the mission can be achieved. It should be emphasised however, that many of

TABLE 1: Pegasus Spacecraft Dry Propulsion Mass (which should by convention also include the 10 tonnes power supply mass, which is in the payload)

System	Mass (tonnes)	Quantity	Final Mass (tonnes)
Nuclear Fission Start Reactor	10	1	10
Reaction Chambers/Ancillaries	10	4	40
Magnetic Field Coils	100	4	400
Laser Driver Radiators	280	4	1,120
Engine Radiators	40.5	4	162
Radiator Coolant (drivers)	87.36	4	349.44
Radiator Coolant (engines)	12.64	4	50.56
Radiator Pumps	40	1	40
Laser Driver System	50	4	200
Beam Lines	2.5	4	10
Diagnostics/Beam Control	0.25	4	1
Induction/Transmission	10	4	40
Pick Up Coil	10	4	40
Power Conversion	10	1	10
Energy Storage	50	1	50
Structural Bars	5	4	20
Insulation Layers	1	4	4
Pumps & Valves	4	1	4
Pellet Injectors	5	4	20
Total			**2,561**

the numbers shown in Table 1 are estimates and not based on a rigorous analysis and so it should be expected that there would be some uncertainty in their value.

Table 2 shows calculations for the different Pegasus Mk2 models explored in this work. Pegasus model (c) is the same as model(a) except that we assume a 99% laser efficiency and this was necessary to close the power cycle and reduce the overall radiator mass [46]. The Pegasus model (c) is the final one put forward by this author. The Pegasus model (b) is for a different pellet mass and pulse frequency. Also shown in Table 2 for comparison is the calculations for a model that is like the Daedalus second engine stage, the basis of the scaling for Pegasus. The energy gain values in the brackets are explained in other papers [30, 46]. The basis for the equations is explained in other publications [51, 52, 53]. For more basic information

TABLE 2: Calculations of Daedalus and Pegasus Propulsion Performance, where the Gain in brackets is the scaled value adopted in the models when closing the Power Cycle

Parameter	Daedalus 2nd	Pegasus (a)	Pegasus (b)	Pegasus (c)
No.Engines	10	4	4	4
Exhaust Velocity (km/s)	9,210	8,897.1	8,668.9	8,897.1
Pellet Mass (mg)	288	72.0	28.8	72.0
Pulse Frequency (Hz)	250	1,000	2,500	1,000
Mass Flow Rate (kg/s)	0.072	0.072	0.072	0.072
Thrust (MN)	0.663	0.64	0.624	0.64
Jet Power (GW)	3,053	2,849.7	2,705.4	2,849.7
Jet Efficiency (%)	90.9	84.9	80.6	84.9
Propulsion Mass (tonnes)	318	2,551	2,551	2,551
Specific Power (MW/kg)	9.604	1.117	1.061	1.117
Driver Energy (MJ)	404	403.1	225.28	147.0
Peak Power (PW)	64.3	907	787	907
Laser Efficiency (%)	99.9	36.1	32.49	99.0
Energy Gain	33.3	23.06 (24.65)	18.82 (20.63)	23.06 (24.65)
Burn-up Fraction (%)	13.3	13.3	13.3	13.3
Output Energy (GW)	13,320	3,587	3,775	3,587

on the fundamental basis of rocket propulsion equations (as distinguished from aircraft propulsion) readers are recommended to read Anderson [54] as an excellent overview.

3 ENERGY DEPOSITION METHOD

3.1 Electron Beams

The fusion engine operates based on laser-induced inertial confinement fusion. This method was chosen as it has a significant experimental basis, but also it was the method adopted for the Project Daedalus study – with the exception that Daedalus used electron beams. We do not adopt electron beams in this work. This is mainly over concerns for the interaction of the different electron beams and the emergence of instabilities. It is important to justify this.

Fig. 8 shows an image given to this author by Alan Bond of an electron discharge experiment, possibly from the 1960s-1970s. It is the understanding that this arrangement is what had partly motivated the design of the Daedalus reaction chamber with its circular electron beam diodes around the circumference. However, there is a problem with this arrangement.

Within the Daedalus engine, a circular series of electron beam diodes would be fired at the target with high repetition [22]. A major problem with this method is that it does not allow for the important requirement to maintain a highly symmetrical implosion geometry, to prevent the growth of hydrodynamic instabilities. The Daedalus appeared to rely on the generation of a corona around the capsule as the surface is ablated [21]. Whilst it is true this corona would be formed, consisting of ions and electrons, it would not propagate any incoming energy around the 4π sphere and so the implosion pressure would be asymmetric.

To solve this, one could instead position electron beam diodes at different positions, such as by using telescopic diodes that ensure there is a 360° coverage of the surface geometry. But now you have a situation where electron beams are coming in from different directions and must transport through the material, and this leads to instabilities.

The two-stream instability is a phenomenon that occurs when an energetic particle stream is injected into a plasma [55]. The charged particles that are contained within the beam will be subject to drift velocities. It is also known as a bump-on-tail instability since it results in a perturbation to the Maxwellian distribution function which defines the velocity of the particles within an ensemble. The two-stream instability prevents two oppositely directed uniform electron beams from passing through each other even if neutralised by a uniform ion background. The instability produces strong spatial inhomogeneities so that the electrons become bunched together and generate an electron plasma wave (high energy electrons) which preheat the fuel.

To show this mathematically, we assume a cold, uniform, unmagnetized plasma with an energetic electron stream injected in, so that a current passes along the plasma and any ions or electrons will have different drift velocities. The electric field E for an electrostatic wave with wavenumber k, and frequency ω is represented with respect to time t and displacement x as:

$$E = E_o e^{i(kx-\omega t)} \tag{6}$$

This leads to a dispersion relation for longitudinal waves with growth rate γ and roots:

$$1 - \omega_{pe}^2 \left[\frac{m_a/m_i}{\omega^2} + \frac{1}{(\omega - kv_o)^2}\right] = 0 \tag{7}$$

$$\omega_j = \omega_j^R + i\gamma_j \tag{8}$$

If the imaginary part is equal to zero, then the solution represents all possible modes with no wave damping or growth.

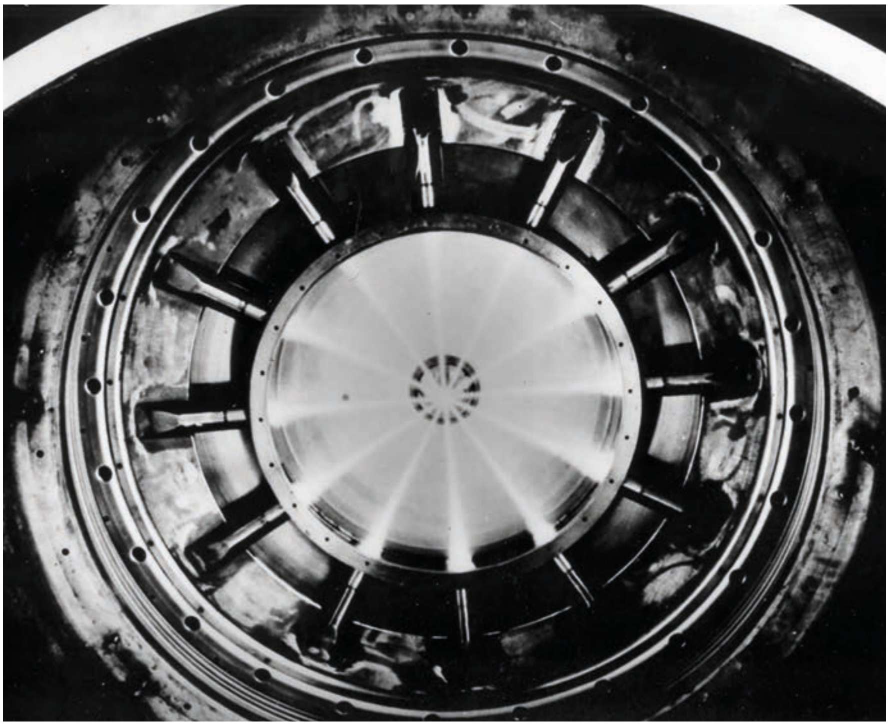

Fig.8 Electron Beam Discharge Experiment *(credit: Alan Bond)*.

But if the imaginary solution is not equal to zero with complex roots it ends up with a second exponential function on the right-hand side for the electric field:

$$E = E_o e^{i(kx-\omega t)} e^{\gamma t} \quad (9)$$

If $\gamma < 0$ then the waves undergo exponential Landau damping. If $\gamma > 0$ then the waves are unstable and grow exponentially, which leads to plasma wave excitation. 1D Particle-In-Cell (PIC) code numerical calculations were performed by this author whilst he was a post-graduate doctoral student at the University of Warwick. These were unpublished calculations but relate to the interaction of counter propagating electron beams within a uniform plasma travelling past each other. Care was taken to ensure sufficient grid points to resolve the wavelength of the unstable modes and sufficient particles per cell to accurately resolve the distribution function.

These were performed for 2, 4 and 6 sets of parallel beams and the results are shown in Fig. 9. The initial conditions were specified as drifting Maxwellian distributions with each beam having a separate particle species but each with the physical properties of an electron. Each species propagates into a plasma of uniform density of 10 particles/m^3 and a uniform temperature of 273 K.

The results of two separate such simulations with counter propagating electron beams are shown in Figure 9 where each image to the right is taken at a different time during the evolution of the beams. The results clearly show the development of the two-stream instability with a growth rate determined by $e^{\gamma t}$ so that the beams become unstable, where the vertical axis is the electron phase space. There is also a large degree of uncertainty associated with the modelling of the physics processes, underlying transport and energy deposition of ultra-high current relativistic electron beams which become unstable during their propagation [56].

Therefore, it is concluded that the proposal for a set of circular positioned electron beams around a reaction chamber in a space propulsion engine for the purpose of initiating ICF implosion poses substantial challenges. This is then a principal objection to the ignition system within the Daedalus propulsion engine.

3.2 Laser Beams

For the Pegasus we have opted to use optical lasers as used in the National Ignition Facility (NIF) and this was one of the early recommendations within Project Icarus by an engineer that had also worked on Project Apollo [57]. This method has a long history of development and experimental achievements. The main reason for this choice was due to experience, and in particular recent experimental results where ignition has been achieved [23, 24, 25], as well as a long legacy of proven experimental developments that even go back to underground tests with the Halite-Centurion programme [58]. Also, the use of optical lasers allows for beam lines which facilitates an ease of positioning around the reaction chamber to encompass the target. Reflecting mirrors on telescoping extension poles can also be used if required to ensure full spherical symmetry. Alternatively, as with the Pegasus, we can adopt a more enclosed reaction chamber that tends more towards an oblate spheroid to facilitate beamline positioning.

Fig. 10(a) shows a schematic that is based on the U.S Nova facility, which was in operation before NIF [29], and here it is mated to a hypothetical propulsion engine. This diagram is shown since one can clearly see all the different parts of the laser system, from the spatial filters, mirrors to the amplifiers and beam spot lines which feed into the target chamber. Essentially for the Pegasus engine shown in Figure 10(b) we are attempting to take a configuration like this and strap it onto the back of the propulsion system and note we have four engines for Pegasus so there would be four separate laser systems.

There are many problems associated with the implementation of this technology, such as the heating and cooling of the optics and the ability to survive in a space environment under intense accelerations. Yet, we must consider that we are talking about the implementation of this technology approximately a century from today and so in between there should be significant technology leaps (i.e. such as in material science) which moves this towards a more realisable state of readiness. Its implementation would also be in parallel with artificial intelligence and so the en-

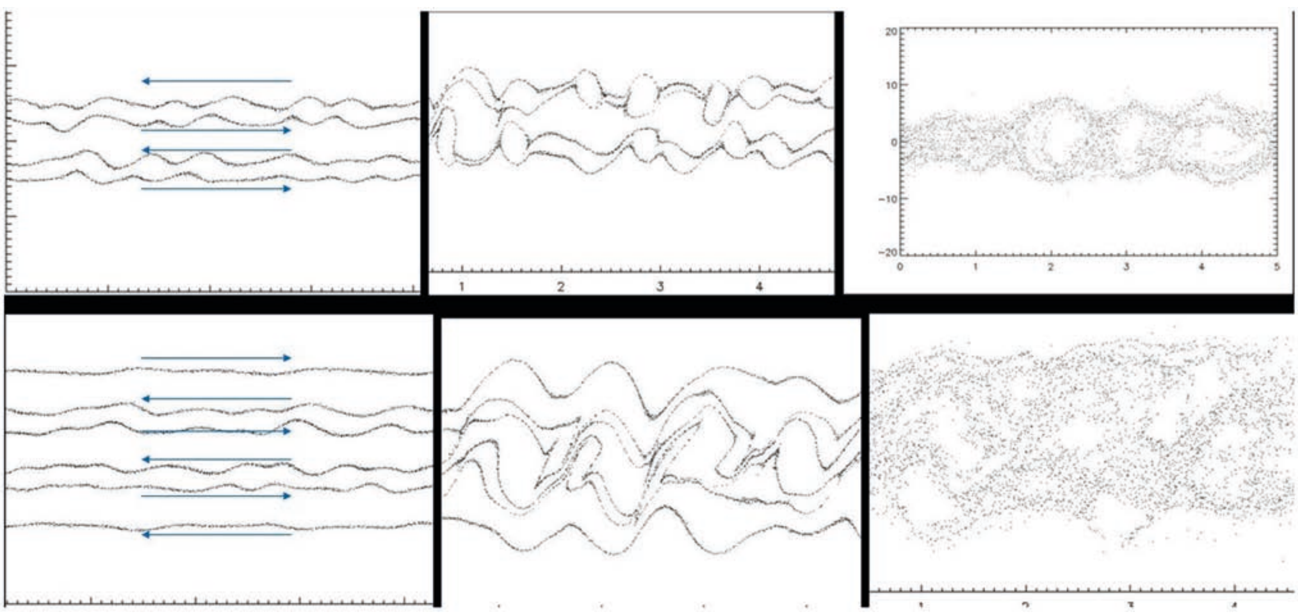

Fig.9 1D PIC Code Simulations of Counter Propagating Electron Beams.

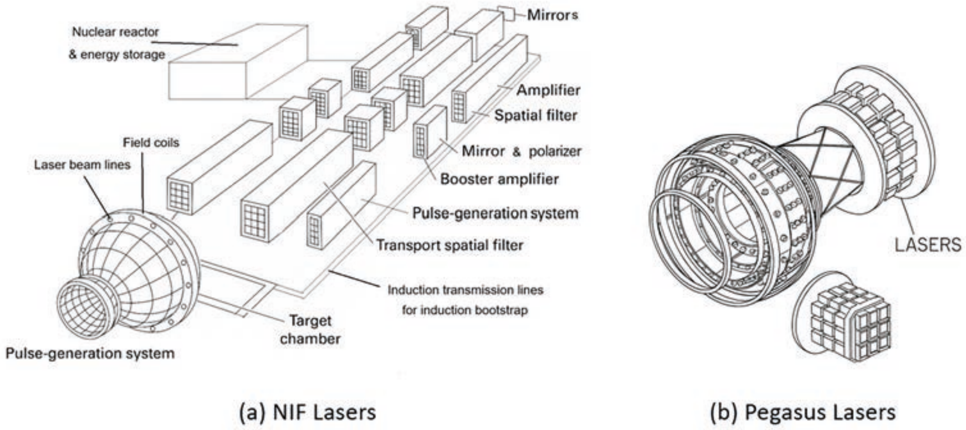

Fig.10 Schematic of a Laser System Integrated with an Engine Reaction Chamber.

tire process of pellet injection, laser firing and alignment would be automated to an incredible degree of accuracy.

For the calculations performed in this work we assumed a hot-spot ignition model for the D^3He target, although as discussed [30], we anticipate the design of the target being more sophisticated. This assumption was made since the calculations are complex and it was a way to simplify them and arrive at a reasonable assessment for the output performance sufficient to allow integration into the propulsion model. We also assume a direct drive system, rather than indirect drive, which would otherwise have the capsule enclosed within a radiation cavity.

Fig. 11 illustrates the illumination of an ICF target by 60 separate laser beam lines where high intensity hot spot regions are generated around the sphere. The laser system adopted for Pegasus would be Nd:glass. However, since this would be initiated at λ = 1,053 nm (1ω) it is necessary to undergo frequency conversion to infrared at λ = 351 nm (3ω) and this involves a frequency conversion loss of around 50%. This means that the total energy generated is significantly reduced. Lasers are defined by the input energy E_{in} (MJ), frequency conversion efficiency ϵ_1 and pulse duration τ_p. The peak power P_{peak} (TW) is then given by:

$$P_{peak} = \frac{\epsilon_1 E_{in}}{\tau_p} \tag{10}$$

Then with a set number of individual beam lines N_{beam} the energy per beam E_{beam} (kJ) and power per beam P_{beam} (TW) is given by:

$$E_{beam} = \frac{\epsilon_1 E_{in}}{N_{beam}} \tag{11}$$

$$P_{beam} = \frac{E_{beam}}{\tau_p} \tag{12}$$

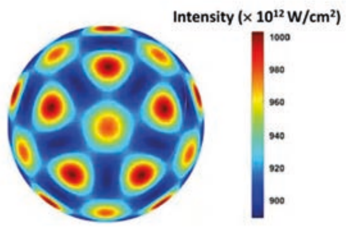

Fig.11 Example Projection of Laser Illumination Pattern onto a Target.

For a pellet outer radius R_{pell} with surface area $A_{pell} = 4\pi R_{pell}^2$, the area of an individual beam line spot size A_{spot} (the area illuminated by a single laser beamline) assuming 100% coverage is given by:

$$A_{spot} = \frac{A_{pell}}{N_{beam}} \tag{13}$$

With the radius of the spot size given as $R_{spot} = (A_{spot}/\pi)^{1/2}$ the laser intensity I_L (Wcm^{-2}) for a direct drive system with multiple beam lines is given by:

$$I_L = \frac{P_{beam}}{A_{spot}} \tag{14}$$

The angular frequency of a laser pulse is given as a function of the wavelength:

$$\omega_L = \frac{2\pi c}{\lambda} \tag{15}$$

The laser intensity can also be related to the energy density ρ (Jcm^{-3}) and the electric field amplitude E_o via:

$$I_L(Wm^{-2}) = c\rho = \frac{c\epsilon_o |E_o^2|}{2} \tag{16}$$

To illustrate the transition of a laser through a material medium, Fig. 12 shows the transport of a laser beam into a plasma of uniform density 0.01 × critical density, where the electric field E_y (V/m) is plotted as a function of the numerical grid position. These calculations were performed by this author using a 1D PIC code [59, 60]. This represents charged particles by pseudo particles and solves the Maxwell's equations for the electric and magnetic field on a finite difference domain known as a Yee grid, with the electric fields having faced centred positions and the magnetic fields being on the edges.

A left-hand boundary condition was imposed as a laser intensity, and the time profile was a representative Gaussian line shape. For the computational domain there were 6,400 grid points and 32,000 particles of species electron and ions each. The right boundary condition describes the plasma outflow as a distribution function. The laser wavelength was 351 nm corresponding to a frequency of 5.38×10^{15} s^{-1} and an electric field amplitude of $E_o = 8.69 \times 10^{10}$ Vm^{-1} for a laser intensity of $I_L = 5.38 \times 10^{15}$ Wcm^{-2}.

As the laser propagates through the material with a given frequency, it will ionise the atoms within the absorber material,

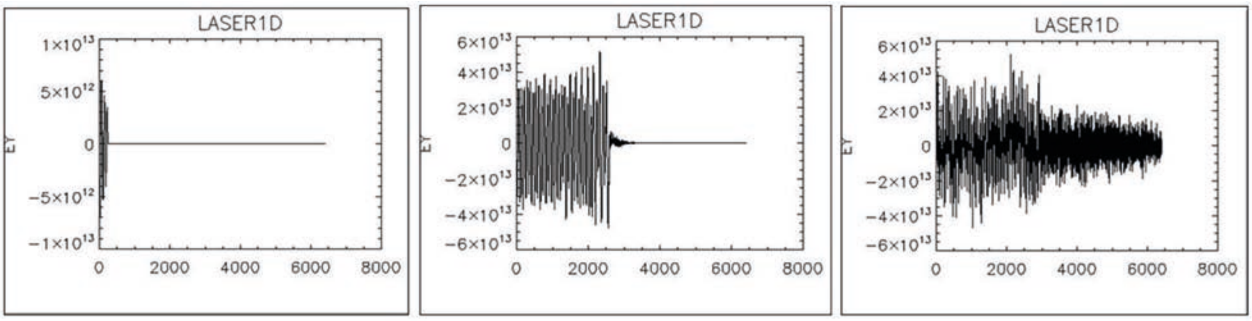

Fig.12 PIC Code Numerical Simulations of the Interaction of a Laser-Plasma.

leading to the generation of an electron cloud (part of what the Daedalus study called a Corona). The electrons will oscillate with an electron plasma frequency which is given as a function of the number density n_e of the electrons by:

$$\omega_{pe} = \sqrt{\frac{n_e e^2}{\epsilon_o m_e}} \approx 56.349\sqrt{n_e} \tag{17}$$

where m_e is the electron mass, e is the electron charge. At some point the frequency of the laser ω will become equal to the frequency of the oscillating electrons within the plasma and this will lead to reflection and scatter of the laser beam. This creates a problem for the propagation of an electromagnetic wave since the implosion of an ICF pellet will depend on the pressure profile generated. The interaction of an electromagnetic wave with a plasma should then satisfy a dispersion relation which is expressed as a function of the wave number $k = 2\pi/\lambda$ and angular frequency $\omega = 2\pi f = 2\pi c/\lambda$ so that the dispersion relation for a plane light wave in a vacuum is:

$$\omega^2 = k^2 c^2 \tag{18}$$

Alternatively, in a non-vacuum the plasma will have a natural frequency of oscillation of the non-propagating charge density in a conducting medium given by the electrons oscillating about the ions at a certain frequency.

$$\omega^2 = \omega_{pe}^2 + k^2 c^2 \tag{19}$$

The electromagnetic wave will only be able to propagate through a plasma provided it has a frequency greater than the electron plasma frequency, i.e. $k^2c^2 \geq \omega_{pe}$. If the laser frequency is less than the electron plasma frequency, then it will not propagate. Within the context of a laser beam interacting with the surface of an ICF pellet this translates from a situation of energy propagation to one of energy absorption and reflection.

In terms of the ICF pellets for the Pegasus design, it was not possible to fully model the interaction of many laser beams onto the surface of individual capsules, but instead we developed a Representative Physics Model (RPM) [30]. This assumes a laser energy deposition as the initial input condition and then the volumetric compression proceeds from there. Table 3 shows the laser beam input assumptions for the different Pegasus models that were eventually adopted in this work. Also shown is the model for the Daedalus second engine stage as a comparison, in terms of what would be required as an energy driver instead of electron beams.

The efficiency of the laser ϵ_{las} can be measured as a function of the energy deposition delivered to the fuel after the losses have been extracted E_{dep} to the ratio of the laser input energy E_{in} that is fired at the target. The engineering efficiency Q_{eng} is compared to the electrical energy E_{ele} at the source (nuclear reactor at start up or from induction loop pulse) prior to taking account of the efficiency rating. These two metrics can be thought of as physics and engineering-based comparisons respectively and are described by:

$$\epsilon_{las}(\%) = \frac{E_{dep}(MJ)}{E_{input}(MJ)} \times 100 \tag{20}$$

$$Q_{las}(\%) = \frac{E_{dep}(MJ)}{E_{ele}(MJ)} \times 100 \tag{21}$$

TABLE 3: Laser Input Parameters for Ignition Physics Models

Design	Daedalus 2nd	Pegasus (a)	Pegasus (b)	Pegasus (c)
m_{cap} (mg)	288	72.0	28.8	72.0
$E_{electrical}$ (MJ)	492.49	403.1	225.28	147.0
E_{input} (MJ)	411	145	73.0	145
λ_o (μm)	1.053	1.05 (1ω)	1.05 (1ω)	1.05 (1ω)
τ_p (ns)	0.00001	0.159	0.093	0.159
P_{peak} (TW)	1.735×10^8	906,250	790,043	906,250
I_L (W/cm^2)	4.905×10^{20}	6.851×10^{16}	8.266×10^{16}	6.851×10^{16}
E_o (V/m)	6.091×10^{13}	7.198×10^{11}	7.907×10^{11}	7.198×10^{11}
N_{beams}	30	50	50	50
E_{dep} (MJ)	333.83	52.35	23.72	143.55
ϵ_{las} (%)	81.22	36.10	32.49	99.0
Q_{eng} (%)	67.79	12.98	10.53	35.61

For the models we assumed a frequency conversion loss (1ω → 3ω) of 95%, energy absorbed into the target outer layers of 5%, energy loss due to the implosion physics of 60%, with the remainder available for fuel energy deposition. So that for the case of an input energy of 145 MJ for example, this was reduced to 137.75 MJ after conversion loss, then down to 130.86 MJ due to outer target absorption, then down to 78.52 MJ due to implosion physics loss, so that 52.35 MJ would be deposited into the fuel. However, for the Daedalus model we assumed 10% energy loss due to the implosion physics, and this was due to the difficulty with trying to get the RPM working with such a large capsule design.

The main problem with lasers like NIF is the very poor efficiencies (typically <1%) and yet for the Pegasus we must assume laser efficiencies that go way beyond the technological state-of-the-art, for even what is envisioned within this paradigm. This then is a major requirement caveat to the design for closure of the model. Indeed, although we assumed an optical laser system for the Pegasus, this turned out to be extremely difficult to implement. For more details, particularly on the high efficiencies adopted, readers should consult the ignition physics paper [30].

In summary, whilst in the modelling for Pegasus we have assumed a Nd:glass optical laser based on experimental validation through NIF, this should not be taken as a firm design decision and instead such a decision would better be made at the time of spacecraft development. There are also other options for energy drivers such as CO_2 lasers, light and heavy ion beam drivers and Krypton Fluoride lasers. For any future successor for Pegasus, a Diode Pumped Solid State Laser (DPSSL) system is likely the preferred choice since there are no hydrodynamic instabilities at high laser intensity. Whilst we have options, the chance of success is high.

4 OPERATION OF PROPULSION ENGINE

Figs 13 and 14 show the engineering design for the propulsion system implemented into the Pegasus spacecraft, but for one engine only (there are four in total). The pellets are injected [61] into the target chamber whilst the laser system fires up and distributes energy through the multiple beam lines, where the positioning of each is carefully selected to ensure simultaneous arrival time at the surface of the pellet. The reaction chamber is an oblate spherical design, that is closed on the inlet end and open on the outlet end. Its shape will be carefully designed to facilitate the accurate positioning of the laser beam lines around the reaction chamber.

The pellet will detonate and generate a large plasma sphere which is made up of charged electrons, ions and electromagnetic radiation. The radiation is either reflected or absorbed into the internal walls, where it is thermalized and can be distributed through the heat management system. Any neutrons generated that escape and are absorbed into the reaction chamber walls will also generate heat and this must be managed. The plasma sphere will interact with the magnetic fields generated by the external field coils so that the charged particles can be reflected rearwards as they follow the magnetic field lines. Most of the energy will be directed rearwards for the purpose of thrust generation, but a small fraction will be extracted for the purpose of powering the next pulse cycle using a pick-up coil and an induced voltage. This is then transmitted down towards an energy storage system and prepared for the next pulse cycle.

The heat generated by the lasers will be distributed through the long horizonal thermal heat radiators that run the length of the vehicle. The heat generated by the engines will be distributed through the fin shaped thermal heat radiators located towards the rear of the vehicle [46].

The fundamental idea is to implode the thermonuclear fuel of the pellet to a state of ignition so that the capsule fuel radius $R(t) \rightarrow 0$. This is achieved using many laser beamlines operating in parallel, ablating the outer surface of the pellet and through momentum conservation it will move inwards putting the fuel under pressure. Many laser beam lines will be needed to achieve this and for Pegasus we assume around 50 separate beamlines.

If we were using a pulse detonation rate of 1 Hz, then this would be one detonation per second. However, since we need to achieve a high acceleration rate a pulse frequency much higher than this must be adopted and by implication the time between detonations is much less than 1 second. This is satisfactory however since the hydrodynamic timescale for the implosion and explosion of each pellet will occur in millionths of a second, 10^{-6} s and the nuclear phase of the ignition will occur in nanoseconds, 10^{-9} s.

For the Daedalus this had a pulse frequency of 250 Hz, so implied a detonation every 0.004 s. However, for Pegasus, the pellet injection - reaction chamber calculations have suggested [61] a pulse frequency requirement of 1,000 Hz and 2,500 Hz for the two different models. This implies that a detonation will occur every 0.001 s and 0.0004 s respectively, which is still much longer than the hydrodynamic time scale for the implosion and explosion of a single pellet. The condition to be satisfied for the time of plasma expansion t_{exp}, and the time between detonations t_{det} and their respective pulse frequencies can be expressed as:

$$t_{exp} < t_{det} = \frac{1}{f_{hz,max}} \Rightarrow f_{hz,max} < \frac{1}{t_{exp}} \tag{22}$$

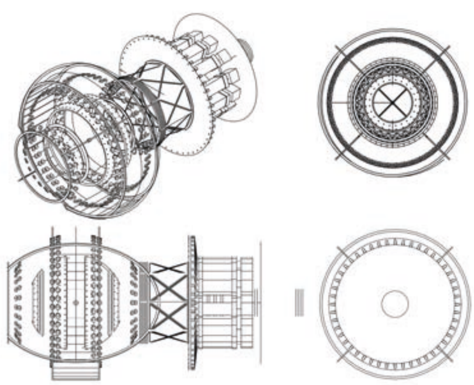

Fig.13 Engineering Schematic of Single Propulsion Engine.

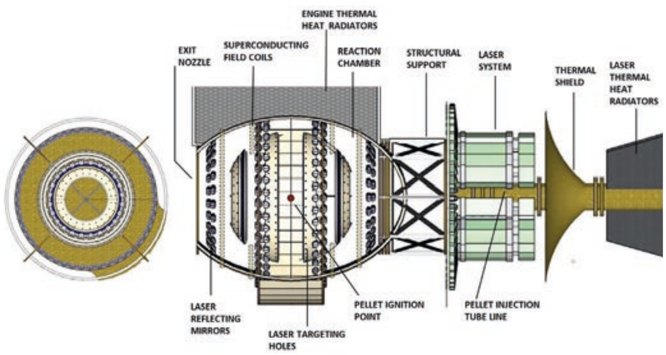

Fig.14 Spacecraft Pegasus Individual Engine.

However, we must also consider the timescale for plasma expansion in the target chamber which depends on the reaction chamber size and is critical to the engineering operation. For Daedalus the expansion speed of the plasma within the reaction chamber was estimated to be $\bar{v}\sim$ 15,000 kms^{-1}. This implies that for Daedalus the two reaction chamber sizes of 50 m (first stage) and 20 m (second stage) that the time for the expansion of the plasma from the detonation point to the chamber walls $t = R/\bar{v}$ would be 3.3 μs and 1.3 μs for the first and second stage respectively. For the Pegasus we are looking at a reaction chamber size in the range R = 5-10 m (based on pellet injection velocity requirements [61] and for the same expansion velocity this would correspond to an expansion time:

$$t_{exp} = \frac{10\,m}{1.5\times10^7} = 0.667\mu s \Rightarrow f_{hz,max} = \frac{1}{6.67\times10^{-7}} \approx 3\times10^6 Hz \qquad (23)$$

$$t_{exp} = \frac{5\,m}{1.5\times10^7} = 0.333\mu s \Rightarrow f_{hz,max} = \frac{1}{3.33\times10^{-7}} \approx 1.5\times10^6 Hz \qquad (24)$$

This is equivalent to 1,500,000 pellets/s and 3,000,000 pellets/s for the 10 m and 5 m reaction chambers respectively. This can be seen as the maximum detonation frequencies. Beyond these frequencies, the plasma from one pellet would still be expanding when the next pellet was ignited, therefore violating the condition, although we are nowhere near this limit for our design.

These times are far smaller than the detonation times and so there should be plenty of time between each detonation so that each plasma ball does not interfere with the next one. With each pellet detonation, the thermonuclear fuel will ignite, and the capsule will begin to disassemble as its radius $R(t) \rightarrow \infty$. A moderate number of neutrons (from secondary and tertiary reactions) and x-rays will be released during this process which may irradiate the spacecraft structure and so require waste heat management. It has been suggested by Yamamura et al [62] that the adoption of a conical shaped target may reduce neutron radiation by attenuation of neutrons from propellant material, which would be a valuable way to reduce shielding mass. Although we did not consider this approach for Pegasus.

The plasma associated with the expanding ball will take on a spherical shape as an isothermal expansion, but since the vehicle is in motion it will be stretched out to form an oblate spheroid and then an entrained spheroid. The repeating sequency of detonations is what will form the collimation (jet) geometry within the engine exhaust, and this is illustrated in Fig. 15.

It is desirable to maintain a well collimated jet as much as possible and to limit the divergence. This is because a conical nozzle design is defined by a correction factor λ_d to the nozzle exit momentum for an ideal rocket [63]. It defines the ratio of the gasses within a finite angle nozzle and the momentum of an ideal nozzle in the axial direction as a function of the half angle θ for the divergence:

$$\lambda_d = \frac{1}{2}(1 + cos\theta) \qquad (25)$$

A nozzle that has little or no divergence will give rise to an efficient axial jet but would require a longer nozzle which increases the mass of the system. A nozzle that has a large divergence angle will have a less efficient performance and lower exhaust velocity (or specific impulse) but also require a shorter nozzle and so lower mass. In any nozzle design a trade between nozzle mass and nozzle efficiency therefore must be made. From this it can be shown [64] that the exhaust velocity is given as a function of the divergence angle term as well as another factor called the momentum weighting factor M_w, burn-up fraction φ and mass defect α, and the speed of light c as follows:

$$v_{ex} = \frac{M_w(2\alpha\phi)^{1/2}c}{2}[1 + cos\theta] \qquad (26)$$

It is useful then to calculate the value of the divergence angle for Pegasus given the two exhaust velocities of 8,897 km/s for model (a) and 8,674 km/s for model (b). Both would have a mass defect of α = 0.0039, burn-up fraction ϕ = 13.3% and a momentum weighting factor M_w = 0.9879 (see reference [64] for description). The divergence half angle is given by:

$$\theta = cos^{-1}\left(\frac{2v_{ex}}{M_w(2\alpha\phi)^{1/2}c} - 1\right) \qquad (27)$$

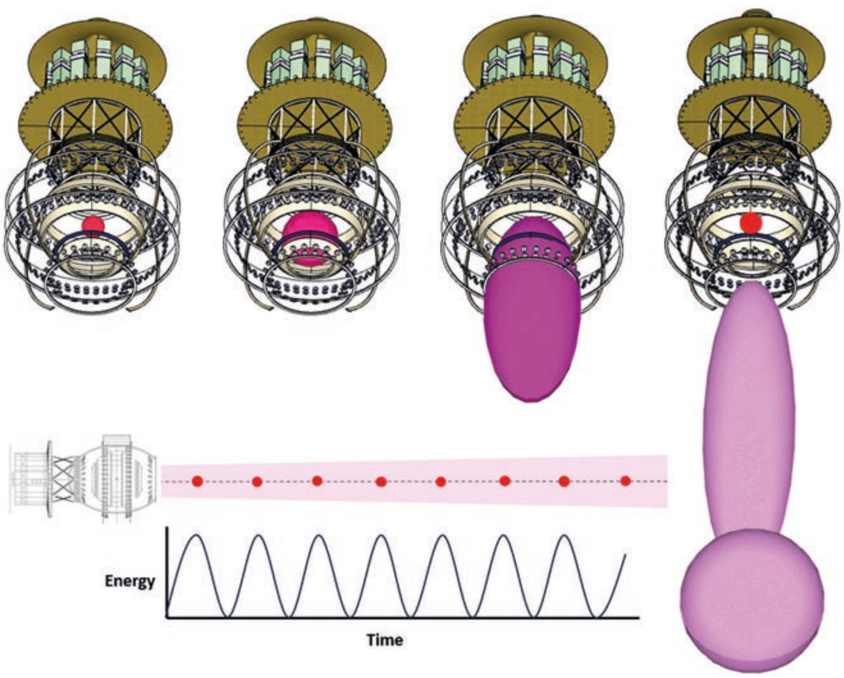

Fig.15 Pulse Detonation of Pellets in Target Chamber.

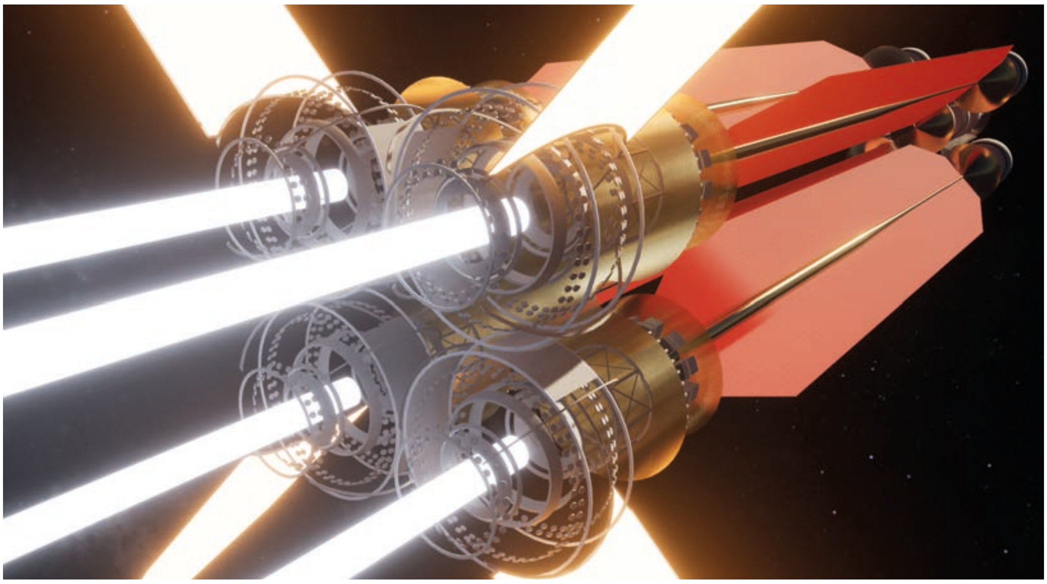

Fig.16 Spacecraft Pegasus with Igniting Engines.

Then when calculating this for the two Pegasus designs, we find the divergence angle to be θ = 30.05° for model (a) and θ = 35.05° for model (b). This is not a surprise given the jet efficiencies of the two designs which are μ_j = 0.849 and μ_j = 0.807 respectively. Thus, compared to Daedalus, Pegasus would appear to be much less efficient in its jet collimation.

For the initial start sequence of the engine a separate nuclear fission reactor will be required to produce the electrical energy sufficient to power the laser arrays. Yet for each detonation some of the energy will be tapped in magnetic pick-up coils which are designed to transmit the electrical energy down transmission lines to power the next pulse cycle. With millions of pellets, it is possible that some underperform or overperform according to the design specification. On this basis it will be necessary for the computer to tailor the energy input of the laser drivers in terms of energy delivered to the target, timing and the shape of the profile. This way, if any diagnostic sensors detect an under/over performance of any given pellet then one of the succeeding pellet detonations can be used to compensate and ensure the trajectory stays within limits. To use an analogy, the targeting of each pellet is like hitting a nail with a hammer, and if the impulse of one hit is under the required force, then the next pulse will hit slightly harder to compensate. This way the energy generated will average out to ensure the required thrust profile.

Figs 16 and 17 illustrate the Pegasus parallel thrust engines under operation during flight. They show a collimated jet exhaust, although the beam is likely to exhibit some degree of divergence. Since any exhaust emission is likely to be in the x-ray part of the electromagnetic spectrum, much of this will be outside of the visible light range, although some of the softer emission might dominate due to the dark background. Contrary to the depiction, it is likely therefore that the engine exhaust will be very light purple or violet in colour. The radiators are also shown to be hot and emitting at slightly different temperatures based on the power rate. In these images the reaction chambers are opened for visibility of internal operation, but they would be fully enclosed except at the exit and surrounded by the magnetic field coils.

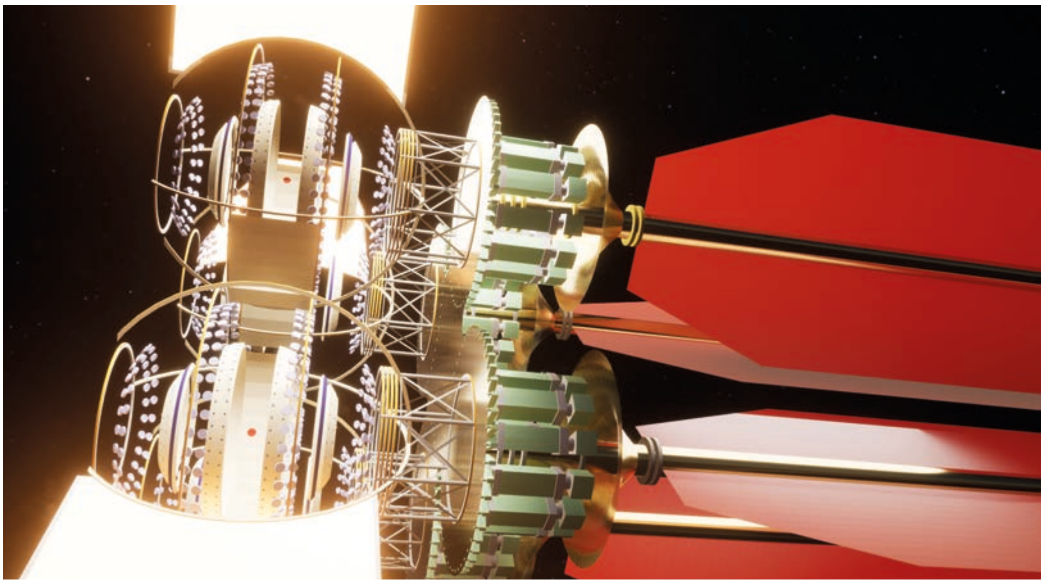

Fig.17 Spacecraft Pegasus Propulsion System Close-Up.

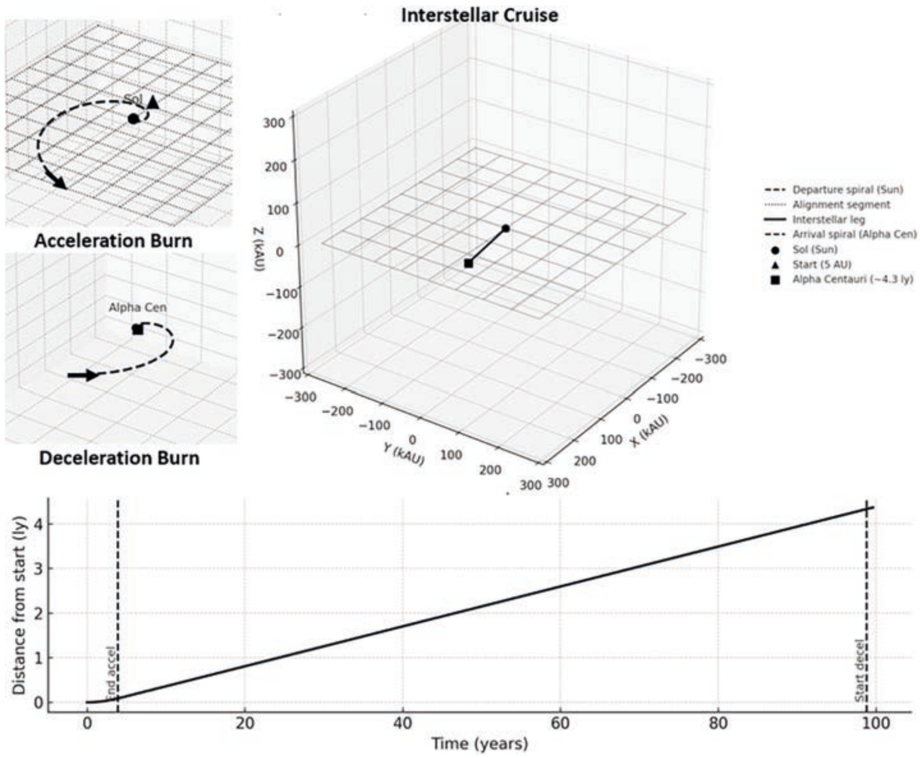

Fig.18 Pegasus Spacecraft Trajectory.

5 TRAJECTORY

The mission of interest involved a spacecraft launch from the vicinity of Jupiter orbit at around 5 AU, from which the spacecraft would accelerate for 3.9 years. It would then cruise for 94.87 years at 4.47%*c*. Following this it would decelerate for 0.86 years to arrive within 1 AU of the target star, Alpha Centauri, at a moderate orbital velocity of 10 km/s. As discussed in [42] we have assumed straight line trajectories and neglected conic sections in this analysis which is standard practice for these sorts of missions and is also adopted by NASA [65].

Fig. 18 show the approximate trajectory of the spacecraft, from a heliocentric position (x = 5, y = 0, z = 0). The spacecraft will spiral out of the ecliptic plane towards the orbital inclination of the target star at an ecliptic latitude of β = 42.6° over the total path length, which is below the ecliptic plane. The spacecraft will head towards the proper motion (0.1° over 100 years) of Alpha Centauri. The acceleration phase therefore involves an orbital plane change as the spacecraft spirals away from the Sun.

For a higher optimisation and accuracy of trajectory one would take into consideration the initial point departure node at Jupiter and early in the thrust profile solar gravity may have a minor influence until the thrust begins to dominate so this would need consideration. In terms of the orbital elements, it would be ideal to ignite the engines near the line of nodes where the outbound line of sight crosses the ecliptic to minimize any thrust out of the plane.

At the destination one might want to consider the collective gravitational potential of Centauri A and B as well as Proxima given they are close. One would also consider the proper motion and radial motion of the target star but also the binary motion of the stellar pair. At low velocity any planetary perturbations at the destination (and during the origin) will need accounting for.

For a trajectory Ω is the Longitude of Ascending Node and ω is the argument of Periapsis. These are two of the key orbital elements to indicate the orientation. We neglect these since we depart from a circular, near-ecliptic (e ≈ 0 staging orbit at 5 AU and then initiate a powered line of sight trajectory and so ω is undefined and Ω is absorbed into the chosen departure epoch. The spacecraft is launched when the node aligns with the direction of the destination target.

In summary, it is argued that all the above are minor corrections to the trajectory and so were neglected for the study. Note that since the spacecraft has a very high velocity, v_c ~13,400 km/s for a 99.64-year mission (~12,000 km/s for 110.29-year mission), the time taken for the trip is well approximated by the simple relation $t = D/v_c$. The only correction is due to relativity but also due to the larger gravitational potential near the origin and target star.

The author has privately demonstrated an original derivation by solving the Euler-Lagrange equation L for the gravitational potential V and kinetic energy K:

$$\frac{d}{dt}\left(\frac{\partial L}{\partial \dot{\theta}}\right) = \frac{\partial L}{\partial \theta} \qquad (28)$$

Where θ is displacement (distance), $\dot{\theta}$ is velocity and $\ddot{\theta}$ is acceleration. Therefore, since $L = K - V$ an equation of motion relative to the origin star M_1 and destination star M_2 is determined to be:

$$\ddot{\theta} = -\frac{GM_1}{\theta^2} + \frac{GM_2}{(D-\theta)^2} \qquad (29)$$

With a relativistic correction as $\ddot{\theta}_{rel} = \ddot{\theta}/\gamma^3$, where γ is the Lorentz factor. This *Interstellar Flight Lagrange* equation is currently under review in a separate publication [66] but justifies the approximations at high velocity in terms of a straight-line trajectory.

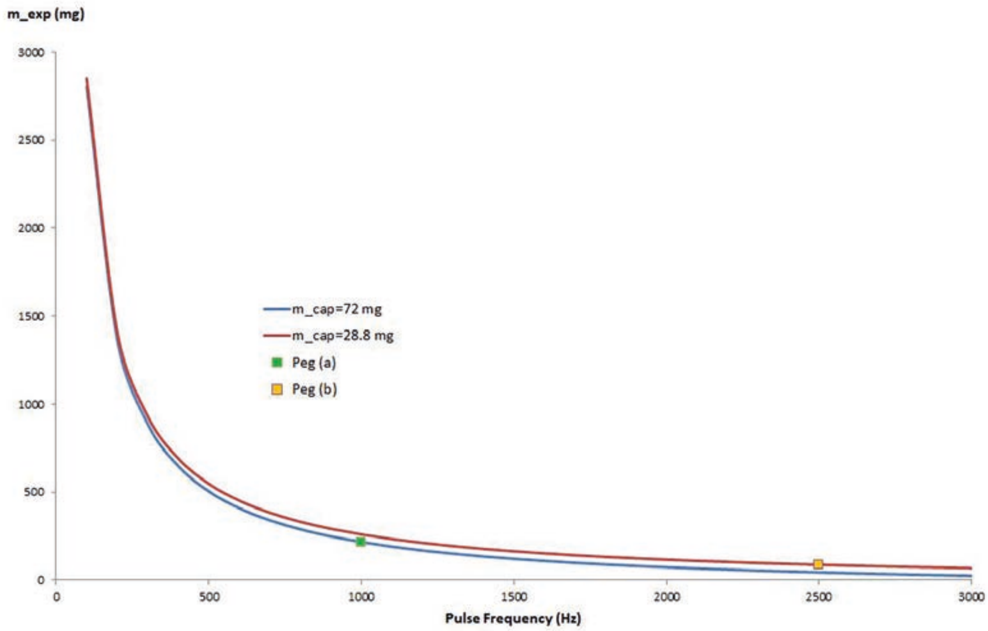

Fig.19 Calculations of Expellant Mass with Pulse Frequency for Thrust Augmentation.

6 THRUST AUGMENTATION

One of the personal aims with Project Icarus was to reduce the overall mass of the system and the propellant mass. We certainly achieved that for a flyby mission, with the *Resolution* design requiring only 2,000 tonnes of propellant compared to the 50,000 tonnes required for Daedalus. However, for the rendezvous design we still have a substantial propellant mass of 43,300 tonnes. This reason this is such an issue is because it is economically expensive to have to mine such a large quantity of fuel and as was shown in the systems engineering paper [42] the helium-3 acquisition was a major component in the capital expenditure model. For this reason, we might consider if there is a way we can further reduce the propellant and we are fortunate that there may be.

As discussed in earlier research it is in fact possible to significantly reduce the thermonuclear fuel requirements for a design using thrust augmentation. This is achieved by increasing the mass flow rate by the injection of expellant material such as hydrogen slush, into the exhaust stream. The thermonuclear plasma will then heat the gas from the expellant and under thermalisation it will reach a higher temperature. This means that you get effectively more material in the exhaust stream and hence enhanced mass flow rate. Although this comes at the cost of reduced exhaust velocity since it has taken heat from the thermonuclear plasma to achieve this state.

Fig. 19. shows a result of calculating the expellant mass requirement as a function of pulse frequency for the two different Pegasus capsule masses of 72 mg and 28.8 mg. Fig. 20 shows the same data but for the change in exhaust velocity expected. These are calculated from the simple relation that $m_{exp} = \frac{\dot{m}}{f_{hz}} - m_{cap}$ but also from the modified exhaust velocity as

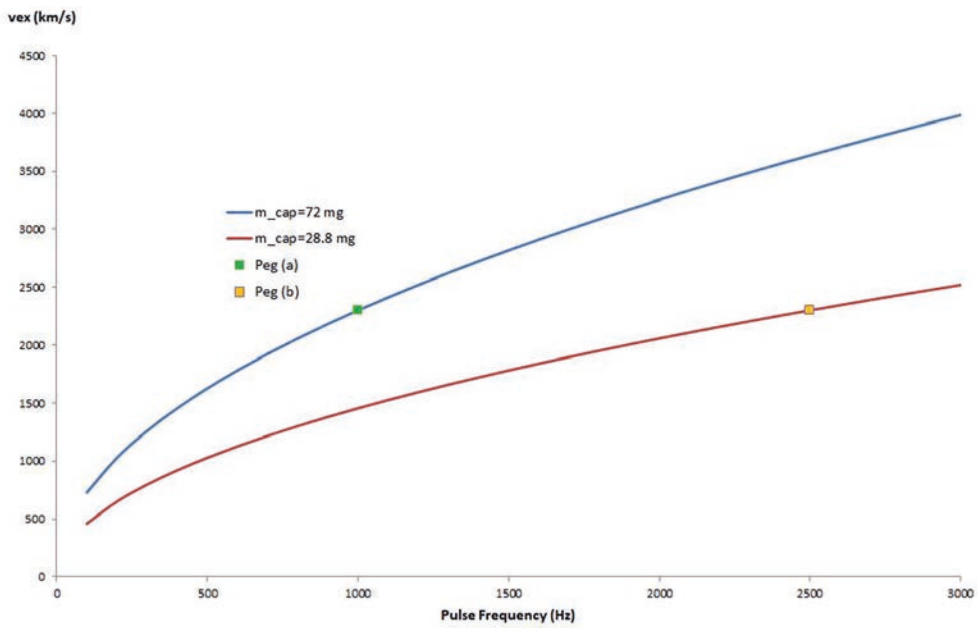

Fig.20 Calculations of Exhaust Velocity with Pulse Frequency for Thrust Augmentation.

described in other work by this author [53], where the exhaust velocity for a non-expellant case and an expellant case are given by the following respectively:

$$v_{ex} = (2\alpha\phi\eta_j)^{1/2} c \qquad (30)$$

$$v_{ex} = \frac{1}{\sqrt{2}}\left[\left(\frac{m_{cap}}{m_{exp}+m_{cap}}\right)\varepsilon_{mix}\alpha\phi\eta_j\right]^{1/2} c \qquad (31)$$

It is interesting that in Fig. 19 we see that the optimum design point, taken where the expellant mass and the pulse frequency are both minimised as a trade, falls on around ~400 → 500 mg and ~400 → 500 Hz. We further note that for the original Daedalus study the pulse frequency was 250 Hz, for which on a lower curve line might correspond to around ~200 → 300 mg pellet mass. The actual pellet masses adopted for the Daedalus second stage was 288 mg and so is in this regime of operation.

Fig. 19 also shows that for a given capsule mass with increased pulse frequency the expellant mass requirement decreases. Fig. 20 shows that for a given capsule mass, with increased pulse frequency the exhaust velocity increases. This sort of chart allows one to visualise what may be possible. The pulse frequency design points for the Pegasus (a) and Pegasus (b) models are shown on the charts.

As an example, Table 4 shows the data points for the two different Pegasus models where we assume m_{exp}/m_{cap} = 3. So that for model (a) with m_{cap} = 72 mg the expellant mass is m_{exp} = 216 g. Similarly for model (b) with m_{cap} = 28.8 mg the expellant mass is m_{exp} = 86.4 g. In both these figures all calculations were based on a set mass flow rate of $\dot{m}$ = 0.288 kg/s. We also assumed φ = 0.133, ε_{mix} = 1.0 (perfect mixing), μ_j = 0.909, α = 0.0039. This leads to a significantly reduced exhaust velocity of just over v_{ex} = 2,300 km/s.

Table 4 shows some example calculations of what may be possible with the use of expellant propellant for thrust augmentation, where the expellant is largely made up of hydrogen slush. The vehicle structure and mass configuration are like the one used for the Pegasus 110-year nominal mission. The calculations assume a constant total propellant mass of 43,200 tonnes, a 4-engine mass flow rate of $\dot{m}$ = 0.288 kg/s, a total acceleration and deceleration burn time of t_b = 4.76 years. For all these calculations we also assume a jet efficiency of μ_j = 0.85. For each of the results they are shown with different ICF capsule mass scaling compared to the Daedalus second stage pellet of m_{cap} = 288 mg.

We see how the exhaust velocity changes with different m_{exp}/m_{cap} ratios but also how the mass of thermonuclear fuel to expellant mass changes and how this influences the mass flow rate, thrust and ultimately time to the destination which is now over several centuries duration due to the reduced velocity increment. Yet this is an option for optimising an interstellar mission for minimum thermonuclear fuel mass, provided we are prepared to accept elongated trip times.

Fig. 21 illustrates how the quantity of expellant mass and thermonuclear fuel mass required changes for different pulse frequencies. For example, we see that for a 28.8 mg fuel capsule at 1,000 Hz, this will lead to 17,293 tonnes thermonuclear fuel and 25,939 tonnes expellant. Similarly, with a much higher capsule fuel mass of 96 mg at 250 Hz, this will lead to 14,411 tonnes thermonuclear fuel and 28,821 tonnes expellant. The profiles converge to a point where $m_{aug} = m_{TN}$ and after this the advantage of using expellant for thrust augmentation becomes less clear, since the motivation is to reduce the thermonuclear fuel required. Ultimately if a spacecraft concept like that shown Fig.22 at the very end of this paper is to become realisable, this may be the sort of design changes that we may need to consider where fusion fuel mass is minimised which then significantly reduces the cost of the mission.

7 CONCLUSIONS

This paper has presented details for the Pegasus spacecraft concept design rendezvous mission as a part of Project Icarus, with emphasis on the propulsion element. We have also revised the concept design to Pegasus *Mk2*, from earlier calculations for the Pegasus *Mk1*. The Pegasus spacecraft is a potential successor to the Daedalus flyby probe spacecraft as a part of this redesign effort.

In particular, the Pegasus addresses several potential issues with the Daedalus design that may have resulted in mission failure. This includes the ICF capsule design, parallelisation of the thrust profile, reduction of total propellant mass (but now for $\approx e^{2\Delta v}$), change of energy driver from electron beams to optical lasers, and the adoption of waste heat radiators to account for probable high energy neutron loss. We note that the use of op-

TABLE 4: Augmented Propellant Case Studies for a Pegasus Mission

Scale	1/4th	1/10th	1/4th	1/10th	1/4th	1/10th
m_{cap} (mg)	72	28.8	72	28.8	72	28.8
m_{exp} (mg)	0.0	3.2	72	115.2	216.0	259.2
m_{exp}/m_{cap}	--	1.5	1.0	4.5	3.0	9.0
m_{TN} (tonnes)	43,200	17,293	21,616	8,646	10,808	32,424
m_{aug} (tonnes)	0	25,939	21,615	34,586	4,323	38,909
f_{hz} (Hz)	1,000	1,000	500	500	250	250
v_{ex} (km/s)	8,897	2,814	3,146	1,989	2,225	1,407
$\dot{m}$ (kg/s)	0.288	0.288	0.288	0.288	2.88	2.88
T (MN)	2.562	0.810	0.906	0.573	6.406	4.051
Δv (km/s)	12,063	3,815	4,265	2,697	3,016	1,907
(%c)	4.02	1.27	1.43	0.89	1.0	0.64
t_{tot} (Yrs)	110	335	300	472	423	666

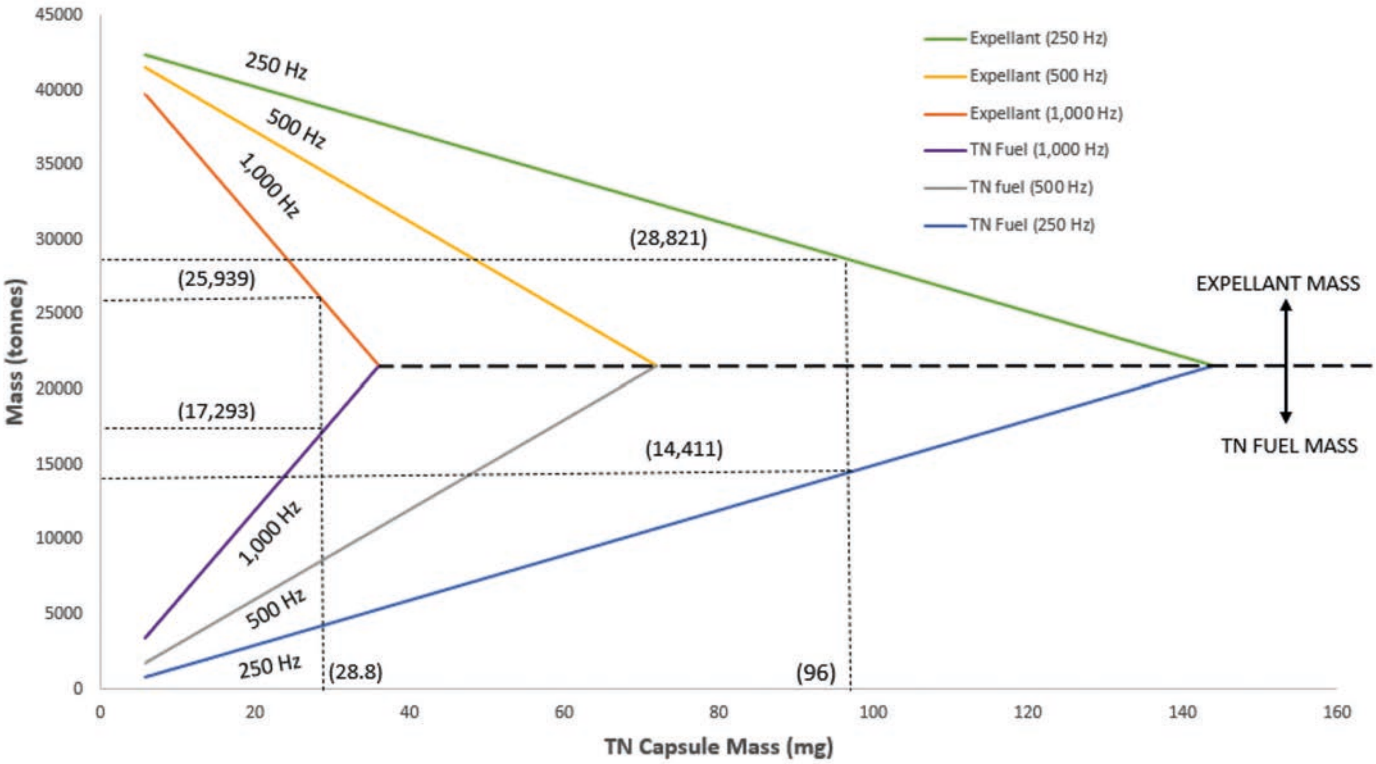

Fig.21 Thermonuclear Fuel versus Expellant Requirement with Pulse Frequency.

tical lasers for laser ignition of an ICF capsule has experimental validation at the National Ignition Facility and with previous underground testing experiments in the Halite-Centurion programme. Although we fully acknowledge the immaturity of the technology for advanced propulsion applications at this time and for the extremely high laser efficiencies specified as a requirement to make these missions possible.

Yet it is a fundamental part of the propulsion system since it is a nuclear pulse engine with each cycle deriving its energy from the previous one. Since we have specified the existence of a substantial neutron flux to the vehicle, this would also necessitate thermalization via spacecraft shielding which we have not examined (although others have [67]), and this would only serve to increase the mass of the spacecraft and perhaps elongate the mission time. Neither have we discussed cryogenic fuel storage and again we would default to the Daedalus approach.

We also highlight that in the design of the thermonuclear ignition of the pellets we set out to be conservative in our approach to claim a limited extrapolation from experiments at NIF. Yet, as detailed in the ignition physics paper [30] we could instead have adopted high energy gain models, and this would have greatly simplified the engineering challenges. Others are invited to indeed take up this challenge and continue to iterate versions of Pegasus assuming different gain models. For this study, it was the goal to provide an assessment of the bottom line, and that is to be found in the tension between the physics and engineering in terms of finding design points of compromise. In the current design of Pegasus, we can see a scenario upon which it might perform and operate as required after significant technology leaps, but we can also see a clear path for substantial improvement in the design, or indeed the adoption of alternative approaches to fusion propulsion [68, 69].

The 150 tonnes payload for Pegasus is delivered to 4.3 *ly* in a trip time of order one century at ~0.046*c* which remains in the target system for several years observation time, must be contrasted with the 450 tonnes payload for Daedalus which is delivered to ~5.9 *ly* in half a century trip time at ~0.122*c*, but with only a few days encounter time to make the required scientific observations.

Perhaps the main achievement here is the demonstration that in principle a rendezvous interstellar mission is feasible, which helps to make the economic case for interstellar probes when considering alternative science programmes such as long-range astronomical observatories which have their value but cannot place technology *in situ* of the target unlike a reconnaissance probe such as proposed here.

We make a statement that the Pegasus must be considered and contrasted with other excellent Project Icarus concept design solutions and collectively they present a design space of options which is reason for high optimism. In addition, we do not claim that we have gone beyond the Project Daedalus Study Group in the level of fidelity and we continue to be in admiration of the quality of that published work from the 1970s, which arguably had its beginnings in even earlier work [47, 70, 71, 72].

For both the Project Daedalus and Project Icarus designs, they represent examples of extreme aerospace design, in terms of the physics and engineering representing the boundary of what is currently possible or in the near future provided our technologies continue to mature. Designing such machines is very challenging and more efforts like this are required if we are to ever become successful in reaching distant worlds yet to be explored. This requires significant investment [73] if they are ever to reach technological readiness [74, 75].

It is this author's hope that the concept design presented here for the Pegasus, is but a foal that may one day grow into a fully matured work horse. For only then will it also grow wings and by that humanity fly to the stars like Bellerophon as he goes to defeat the Chimera - which we might see as a metaphor for the physics and engineering challenges we face to realise such a dream. Indeed, before we can make the journey vehicles like Pegasus must be tamed and this requires the efforts of a multi-generational scientific endeavour inspired by the vision of the stars. Ultimately, Pegasus is just one of the many possible solutions towards achieving interstellar flight over the next century that goes even beyond fusion [76, 77]. This only makes such missions more credible as a part of our realistic future in space.

Acknowledgements

The author would like to thank Rob Swinney, Robert Freeland and Michel Lamontagne for discussions in relation to the Pegasus spacecraft concept design. Michel is also acknowledged for producing some of the awesome three-dimensional graphical visuals for the Pegasus spacecraft design and he has earned his rightful place to be called a Graphical Engineer.

REFERENCES

1. K. F. Long, M. Fogg, R. Obousy, A. Tziolas, A. Mann, R. Osborne, A. Presby, "Project Icarus: Son of Daedalus – Flying Closer to Another Star", *JBIS*, **62**(1/12), 403-414, 2009.
2. K. F. Long, M. Fogg, R. Obousy, A. Tziolas, A. Presby, A. Mann, R. Osborne, "Project Icarus: Terms of Reference Document", Internal Document, 4 November 2009.
3. K. F. Long, R. K. Obousy, "Project Icarus: Project Programme Document (PPD) – Overview Project Plan Covering Period 2009 2014, Incorporating Major Task Plan for Phase III Concept Design Covering Period May 2010 – April 2011", Internal Report, Published 12 May 2010.
4. K. F. Long, R. Obousy, A. Tziolas, "Project Icarus: The Origins and Aims of the Study", *JBIS*, **64**(3), 88-91, March 2011.
5. A. Bond, A. Martin, "Project Daedalus: The Mission Profile", Final Study Report, *JBIS*, Special Supplement, S37-S42, 1978.
6. A. R. Martin, "Project Daedalus: The Evidence for Planetary Companions of Barnard's Stars", Project Daedalus, Final Report, *JBIS*, Special Supplement, S19-S23, 1978.
7. R. J. Halyard, "Optimum Interstellar Travel Times for Pulsed Fusion Propulsion Systems", *JBIS*, **44**, 377 - 384, 1991.
8. A. R. Martin, A. Bond, "Nuclear Pulse Propulsion: A Historical Review of an Advanced Propulsion Concept", *JBIS*, **32**(8), 283-310, August 1979.
9. A. Bond, A. R. Martin, "Project Daedalus Reviewed", *JBIS*, **39**, 385-390, 1986.
10. R. W. Swinney, R. M. Freeland, M. Lamontagne, "Project Icarus: Designing a Fusion Powered Interstellar Probe", *Acta Futura*, **2**, 47-49, 2020.
11. R. S. Swinney, R. Freeland, M. Lamontagne, K. F. Long, "Project Icarus: A Review of the Project, Spacecraft Concepts and Design Process, *JBIS*, **78**(05), 143-154, May 2025. DOI https://doi.org/10.59332/jbis-078-05-0143.
12. R. M. Freeland, "M. Lamontagne, Firefly Icarus: An Unmanned Interstellar Probe using Z-Pinch Fusion Propulsion", *JBIS*, **68**(3/4), 68-80, Mar-Apr 2015.
13. R. M. Freeland, "Plasma Dynamics in Firefly's Z-Pinch Fusion Engine", *JBIS*, **71**(8), 288-293, Aug 2018.
14. R. M. Freeland III, "Project Icarus: Firefly, An Unmanned Interstellar Probe using Z-Pinch Fusion Propulsion (Final Design)", *JBIS*, 2025.
15. M. Stanic, J. T. Cassibry, R. B. Adams, "Project Icarus: Analysis of Plasma Jet Driven Magneto-Inertial Fusion as Potential Primary Propulsion Driver for the Icarus Probe", *Acta Astronautica*, **86**, 47-54, May-June 2013.
16. M. Stanic, "Project Icarus: Ultra-Dense Deuterium Based Vehicle Concept", Internal Team Design Report, 11 December 2013.
17. K. F. Long, "Project Icarus: Development of Fusion Based Space Propulsion for Interstellar Missions", *JBIS*, **69**, 289-294, 2016.
18. J. D. Lawson, "Some Criteria for a Power Producing Thermonuclear Reactor", Technical Report for the Atomic Energy Research Establishment, Harwell, England, UK, AERE GP/R 1807, December 1955.
19. N. R. Schulze, "Fusion Energy for Space Missions in the 21st Century", NASA TM4298, August 1991.
20. J. Cassibry, R Cortez, M Stanic et al., "Case and Development Path for Fusion Propulsion", *Journal of Spacecraft and Rockets*, **52**(2), 595-612, 20 Jan 2015.
21. A. Martin, "Project Daedalus: The Propulsion System Part I, Theoretical Considerations & Calculations", *JBIS*, Special Supplement, S44-S62, 1978.
22. A. Bond, A. R. Martin, "Project Daedalus: The Propulsion System Part II, Engineering Design Considerations", *JBIS*, Special Supplement, S63-S82, 1978.
23. A. B. Zylstra, O. A. Hurricane, D. A. Callahan, et al., "Burning Plasma Achieved in Inertial Fusion", *Nature*, **601**(7894), 542-548, 2022.
24. A. B. Zylstra, A. L. Kritcher, O. A. Hurricane, et al., "Experimental Achievement and Signatures of Ignition at the National Ignition Facility", *Physical Review E*, **106**, 025202, August 2022.
25. A. R. Christopherson, O. A. Hurricane, C. Weber et al., "Alpha-Heating Analysis of Burning Plasma and Ignition Experiments on the National Ignition Facility", *Physics of Plasmas*, **30**(6), 062705, June 2023.
26. B. Bishop, "National Ignition Facility Achieves Fusion Ignition", 14th December 2022. https://www.llnl.gov/news/national-ignition-facility-achieves-fusion-ignition [last accessed 1 April 2023]
27. C. Orth, "VISTA – A Vehicle for Interplanetary Space Transport Applications Powered by Inertial Confinement Fusion", UCRL-TR110500, 2003.
28. S. P. Pfalzner, *An Introduction to Inertial Confinement Fusion*, Taylor & Francis, 2006.
29. J. D. Lindl, *Inertial Confinement Fusion, The Quest for Ignition and Energy Gain Using Indirect Drive*, Springer, AIP Press, 1998.
30. K. F. Long, "Project Icarus: The Pegasus Spacecraft Inertial Confinement Fusion Ignition Physics Design", *JBIS*, **78**(10), 344-368, October 2025. DOI https://doi.org/10.59332/jbis-078-10-0344
31. K. F. Long, "Project Icarus: Nuclear Fusion Space Propulsion and the Icarus Leviathan Concept", *Space Chronicle*, **65**(1), 2012.
32. K. F. Long, "Application of the HeliosX ICF Advanced Propulsion Mission Analysis Code to Perturbed Interstellar Design Models", *JBIS*, **76**(3), 370-380, March 2023. DOI: https://doi.org/10.59332/jbis-076-03-0094
33. K. F. Long, "Development of the HeliosX Mission Analysis Code for Advanced ICF Space Propulsion", *Acta Astronautica*, **202**, 157-173, January 2023.
34. "HeliosX, "A Numerical Modelling Tool for Designing Fusion-Powered Spacecraft", *Research Futures*, **151**, February 2024.
35. K. F. Long, "On the Application of Pulse Propulsion Frequency in Inertial Fusion Space Mission Design", *JBIS*, **75**(4), 127-141, April 2022.
36. K. F. Long, "Interstellar Propulsion using Laser Driven Inertial Confinement Fusion Physics", *Universe*, **8**(8), 421, 15 August 2022.

37. K. F. Long, "Sunvoyager: A Concept Mission for a 1,000 AU Interstellar Precursor Probe Driven by ICF Propulsion", *Journal of Spacecraft & Rockets*, **60**(3), May/June 2023.

38. K. F. Long, "Development of the SunVoyager Interstellar Precursor Probe Driven by Inertial Confinement Fusion Propulsion", *Journal of Spacecraft & Rockets*, 28 May 2024.

39. K. F. Long, "Discovery-III: Missions to the Outer Planets using Inertial Confinement Fusion Propulsion", *Journal of Spacecraft & Rockets*, **28** January 2025.

40. C. H. Williams, S. K. Borowski, "An Assessment of Fusion Space Propulsion Concepts and Desired Operating Parameters for Fast Solar System Travel", *33rd AIAA/ASME/SAE/ASEE Joint Propulsion Conference & Exhibit, AIAA 97-3074, 6-9 July 1997*.

41. C. D. Orth, P J Turchi, S A Carpenter, J F Santarius, R H Frisbee, C H Williams, "Recommended Design Practices for Conceptual Nuclear Fusion Space Propulsion Systems", *Special Project Report, SP-108-2004, AIAA, 2004*.

42. K. F. Long, "Project Icarus: The Pegasus Spacecraft Concept Design Engineering Systems Description", *JBIS*, **78**(6), 186-205, June 2025, DOI https://doi.org/10.59332/jbis-078-06-0186

43. R. Osborne, M. Lamontagne, "Project Icarus: Secondary Nuclear Power", *JBIS*, 2025.

44. R. Osborne, M. Lamontagne, "Project Icarus: Systems Architecture", *JBIS*, 2025.

45. R. Osborne, M. Lamontagne, "Project Icarus: Vehicle Systems", *JBIS*, 2025.

46. K. F. Long, "Project Icarus: The Pegasus Interstellar Spacecraft Propulsion Power Cycle", JBIS, **78**(10), 330-343, October 2025. DOI https://doi.org/10.59332/jbis-078-10-0330

47. L. Shepherd, "Interstellar Flight", *JBIS*, **11**, 149-167, 1952.

48. T. A. Heppenheimer, "Some Advanced Applications of a 1-Million Second I_{sp} Rocket Engine", *JBIS*, **28**, 175-181, 1975.

49. C. Powell, "Flight-Time Minimisation for an Energy-Limited Flyby Star Probe", *JBIS*, **27**(4), 267-272, April 1974.

50. R. A. Hyde, "A Laser Fusion Rocket for Interplanetary Propulsion", Paper IAF-83-396, *34th International Astronautical Congress, Budapest, October 1983*.

51. K. F. Long, R Obousy, A Hein, "Project Icarus: Optimisation of Nuclear Fusion Propulsion for Interstellar Missions", *Acta Astronautica*, **68**, 1820-1829, 2011.

52. K. F. Long, "Project Icarus: Specific Power for Interstellar Missions using Inertial Confinement Fusion Propulsion", *JBIS*, **69**, 190-194, 2016.

53. K. F. Long, "Minimum Condition Requirements in Laser Driven ICF for Advanced Space Propulsion Applications", *JBIS*, **77**(1), 23-32, January 2024. DOI: https://doi.org/10.59332/jbis-077-01-0029

54. J. D. Anderson, *Introduction to Flight*, Third Edition, McGraw-Hill International Editions, 1989.

55. W. L. Kruer, "The Physics of Laser Plasma Interactions", *Frontiers in Physics*, Westview Press Books, 2003.

56. R. G. Evans, "Modelling Electron Transport for Fast Ignition", *Plasma Phys.Control.Fusion*, **49**, B87-B93, 2007.

57. J. R. French, "Project Icarus: A Review of the Daedalus Main Propulsion System", *JBIS*, **66**(7/8), 248-251, July/August 2013.

58. J. D. Lindl, "Development of the Indirect-Drive Approach to Inertial Confinement Fusion and the Target Physics Basis for Ignition and Gain", *Physics of Plasmas*, **2**(11), 3933, 1995.

59. T. D. Arber, K. Bennett, C. Brady, "Contemporary Particle-In-Cell Approach to Laser-Plasma Modelling", *Plasma Phys. Control. Fusion*, **57**, 113001, 2015.

60. C. Brady, *Epoch, An Open Source PIC Code Developed for High Energy Density Physics*, University of Warwick, 2014.

61. K. F. Long, M. Lamontagne, "Project Icarus: Pellet Injection System for the Pegasus Spacecraft Concept Design", *JBIS*, **78**(6), 206-215, June 2025, DOI https://doi.org/10.59332/jbis-078-06-0206

62. T. Yamamura, M. Edamoto, T. Kojima, T. Morita, N.Yamamoto, A. Sunahara, T. Johzaki, H, Nakashima, "Numerical Analysis on a Conical Shaped Target for Laser Fusion Rocket", *High Energy Density Physics*, **37**, 100894, 2020.

63. G. P. Sutton, O. Biblarz, *Rocket Propulsion Elements*, Seventh Edition, John Wiley & Sons, 2001.

64. K. F. Long, "Operational Performance Parameter Range in ICF Propulsion Theory", *Acta Astronautica*, 2010, 303-310, May 2023.

65. C. H. Williams, L. A. Dudzinski, S. K. Borowski, A. J. Juhasz, "Realizing 2001: A Space Odyssey: Piloted Spherical Torus Nuclear Fusion Propulsion", NASA/TM-2005-213559, *AIAA-2001-3805, March 2005*.

66. K. F. Long, *Stellar Engines: Advanced Spacecraft Propulsion through Extreme Aerospace Engineering Design*, Springer, 2026.

67. P. Birch, "Radiation Shields for Ships and Settlements", *JBIS*, **35**(11), 515 - 519, November 1982.

68. T. Kammash, "Self-Fueling Fusion Hybrid Reactor for Space Power and Propulsion", *JBIS*, **63**(9/10), 384-386, September/October 2010.

69. G. H. Miley, X. Yang, K. A. Flippo, H. Hora, "Fusion Space Propulsion using Fast-Ignition Inertial Confinement Fusion (FI-ICF)", *JBIS*, **63**(9/10), 387 - 390, Sep/Oct 2010.

70. A. Bond, "Problems of Interstellar Propulsion", *Spaceflight*, **13**, 245-251, 1971.

71. F. Winterberg, "Rocket Propulsion by Thermonuclear Microbombs ignited with Intense Relativistic Electron Beams", *Faumfahrtforschung*, **15**, 208-217, 1971.

72. G. Dyson, *Project Orion – The Atomic Spaceship 1957-1965*, The Penguin Press, 2002.

73. K. F. Long, "Project Icarus: The First Unmanned Interstellar Mission, Robotic Expansion & Technological Growth", *JBIS*, **64**, 107-115, 2011.

74. J. C. Mankins, "Technology Readiness Levels", A White Paper, NASA, 1995.

75. G. R. Schmidt and M. J. Patterson, "In-Space Propulsion Technologies for the Flexible Path Exploration Strategy", Presented *61st IAC Prague, IAC-10.C4.6.2, 2010*.

76. E. Mallove, G. Matloff, *The Starflight Handbook, A Pioneer's Guide to Interstellar Travel*, John Wiley & Sons Inc, 1989.

77. K. F. Long, *Deep Space Propulsion, A Roadmap to Interstellar Flight*, Springer, 2011.

Received 30 July 2025 **Approved** 3 October 2025

Fig.22 (overleaf) Spacecraft Pegasus in the Deep Interstellar Medium. *(credit: Michel Lamontaigne)*

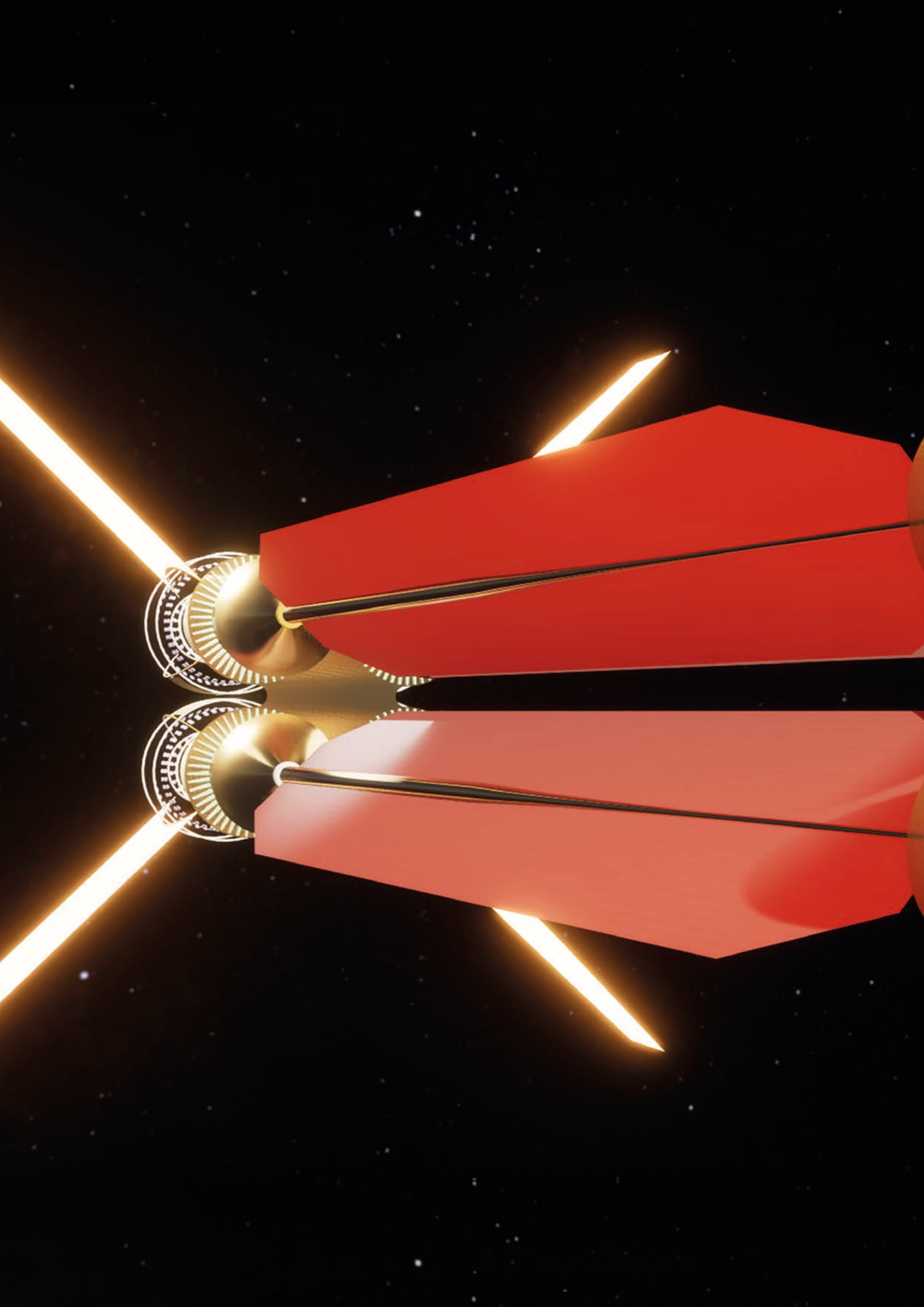

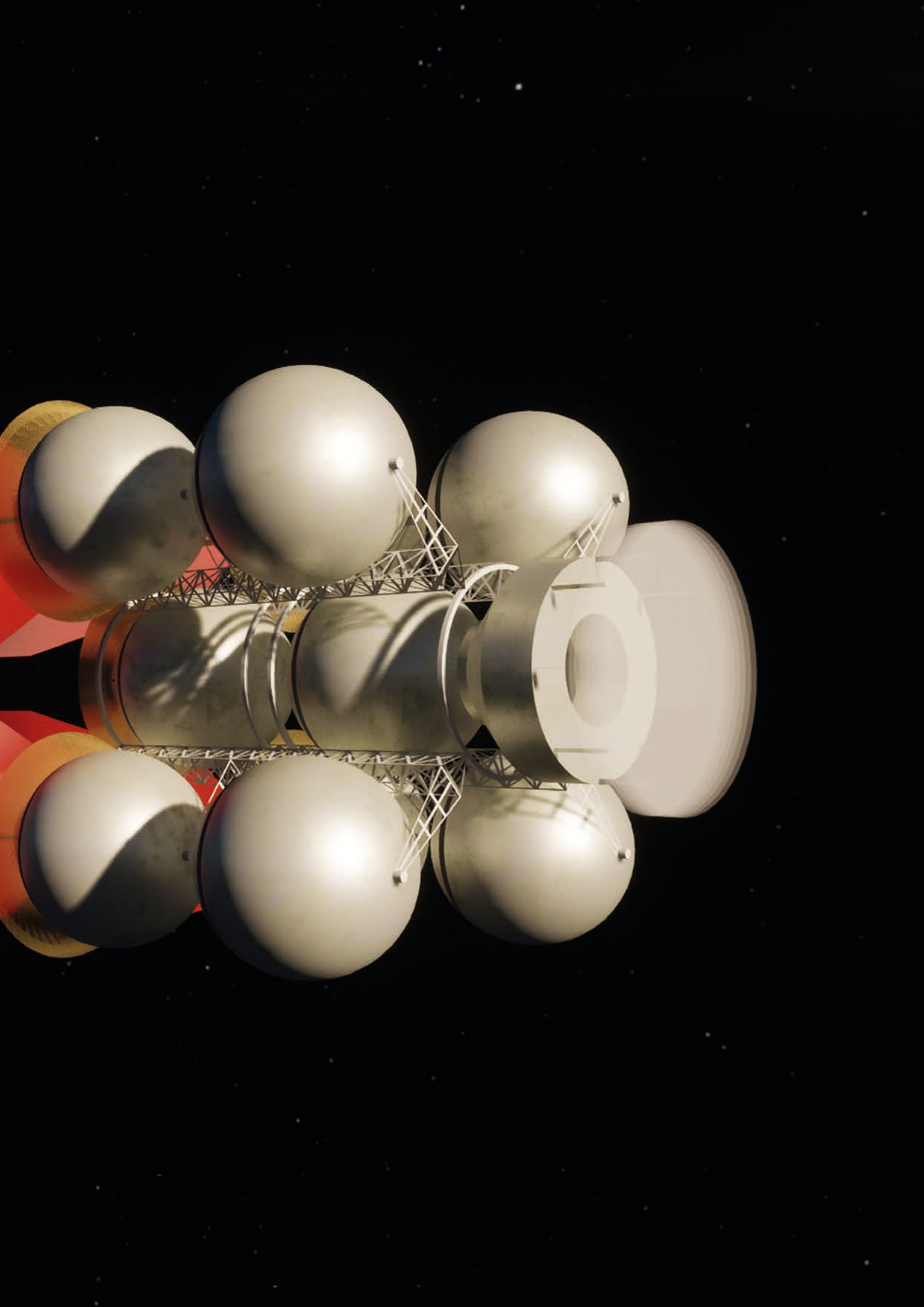

Project Icarus: The Pegasus Spacecraft Concept Design ICF Propulsion for an Interstellar Rendezvous Mission – Part B

K. F. LONG Interstellar Research Centre, Stellar Engines Ltd, 65 Peach Street, Wokingham, RG40 IXP, United Kingdom

Email interstellarresearchcentre@gmail.com

DOI https://doi.org/10.59332/jbis-078-12-0422

This paper is a follow-up to an earlier one in relation to the design of an interstellar spacecraft called Pegasus, which set out to re-design the Daedalus spacecraft based on advances in science and technology. The Pegasus is an inertial confinement fusion propelled spacecraft driven by laser beams, the technology for which is now supported by successful experiments at the National Ignition Facility. The Pegasus is a concept for an interstellar rendezvous mission carrying a 150 tonnes payload to 4.3 *ly* in a trip duration of order a century. In this paper we discuss various physics and engineering issues relevant to the propulsion system, to include the reaction chamber, magnetic field control and charged particle jet collimation. This paper is a final contribution to Project Icarus.

Keywords: Interstellar Studies, Fusion Propulsion, Pegasus, Project Icarus

1 INTRODUCTION

Project Icarus is a theoretical design study first initiated in 2009 which set out to design an interstellar probe [1, 2, 3]. It was based on the British Interplanetary Society Project Daedalus study [4], an interstellar flyby probe carrying a 450 tonnes payload to be sent to Barnard's star 5.9 *ly* away in a total trip time of order half a century (originally it was defined as a 40-year mission). Project Icarus sets out to design an interstellar rendezvous probe carrying 150 tonnes payload mass to 4.3 *ly* in a trip time of order one century.

Fig. 1 shows an illustration of the overall propulsion system used in the Pegasus design. This involves many different technologies all of which would have to achieve maturation before entering operation. We acknowledge the complexity of this challenge. In a separate paper [5], the use of this propulsion system to propel the Pegasus spacecraft to its interstellar target was discussed. Two separate mission profiles were shown and here we focus briefly on the one that is less than one century per the Project Icarus mission requirement.

In an earlier paper we discussed the propulsion system for the Pegasus spacecraft [6]. In this second half we discuss some of the critical physics issues relevant to the propulsion system such as the plasma beta, Larmor radius and expansion of the plasma within the reaction chamber. We also discuss collimation of the plasma jet which is made up of charged particles to include in a four-engine parallel thrust configuration. We also discuss the reaction chamber mass, volume and geometry. Finally, we discuss the magnetic field coils that are so necessary to direct the charged particles for thrust generation.

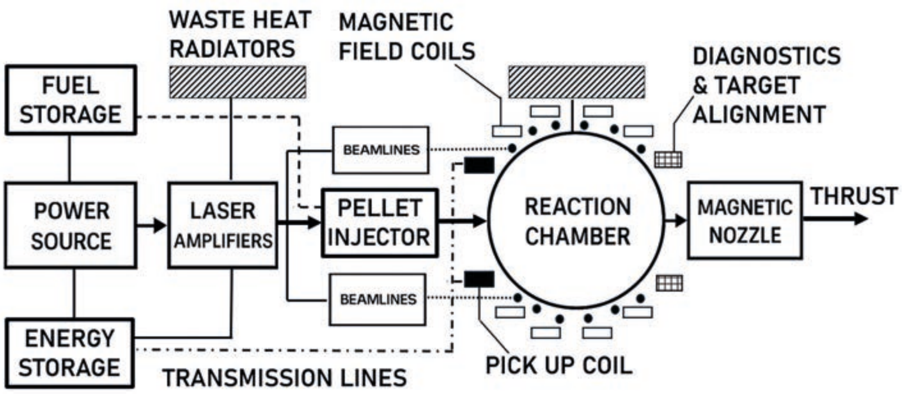

Fig.1 Engineering Block Diagram for Propulsion System.

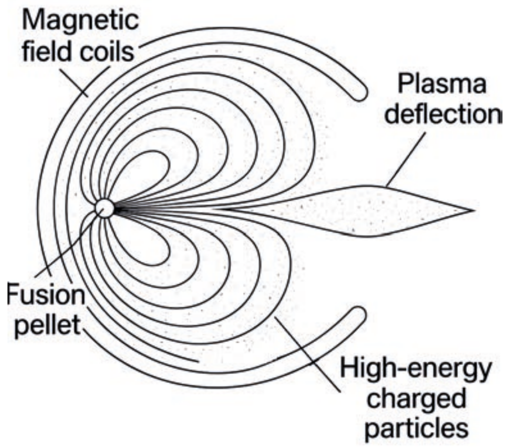

Fig.2 Thermal Expansion of Charged Particles in Magnetic Nozzle.

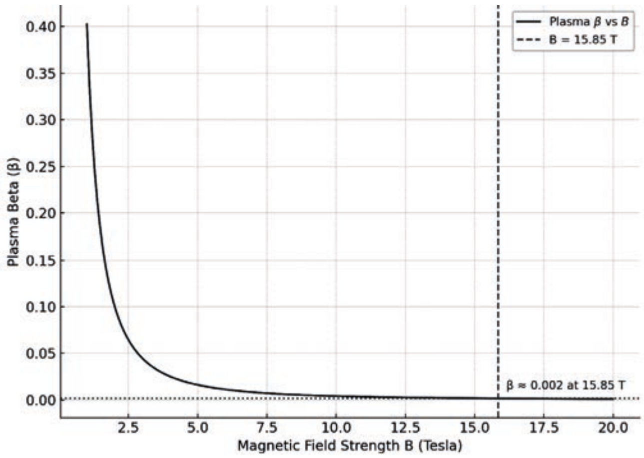

Fig.3 Plasma Beta vs Magnetic Field Strength for a Magnetic Nozzle.

2 PROPULSION PHYSICS

2.1 Plasma Beta

As illustrated in Fig. 2, a magnetic nozzle will be required for the purpose of directing the charged particles within the thermonuclear generated plasma exhaust rearwards for thrust generation. The engine will operate like the Daedalus engine in the use of superconducting lines around the chamber which have the function of generating a strong magnetic field. The magnetic fields maintain a separation distance between the reaction chamber walls and the maximum distance for which the charged particles are expected to spiral to within their gyroradius of circular motion around the path of a field line. If the gyroradius reaches as far as the wall, then the plasma will contact the material structure leading to significant heating. The critical point where the thrust is enabled is when the plasma beta $\beta_B \rightarrow 1$ around a deflection point so that the charged particles are pushed outwards away from the reaction chamber.

The plasma beta is given as the ratio of the plasma pressure P_p to magnetic pressure P_B, which are given respectively by:

$$P_p = nk_B T \tag{1}$$

$$P_B = \frac{B^2}{2\mu_o} \tag{2}$$

Therefore:

$$\beta_B = \frac{2nk_B\mu_o T}{B^2} \tag{3}$$

Where $k_B = 1.38 \times 10^{-23}$ J/K is the Boltzmann constant and $\mu_o = 1.256 \times 10^{-6}$ N/A^2 is the permeability of free space. The plasma beta will be lower with a stronger magnetic field, but it also depends on the number density of charged particles and the temperature of the plasma. If the field strength is not sufficiently high, then the particles will spiral back around and interact with the material structure.

Fig. 3 shows a calculation for the value of the plasma beta as a function of different magnetic field strengths, where the value for the Daedalus study of 15.85 T is included (see later discussion). This plot was generated assuming a T = 10 keV plasma with a number density of $n = 10^{20}$ m^{-3} which might be typical in a magnetic nozzle of this type. For 15.85 T, we find that $\beta \approx 0.002$ or 0.2%.

Essentially for $\beta_B < 1$, where $P_P < P_B$, we have a strong external magnetic field which controls the plasma, the magnetic pressure dominates, and this is a stable configuration. For $\beta_B = 1$, where $P_P = P_B$, the two pressures are comparable, and we have a release point, but it is also optimum for performance. For $\beta_B > 1$, where $P_P > P_B$, we have a weak external field and the plasma will diverge, since the plasma pressure dominates and any magnetic confinement becomes unstable.

It is practical to express the plasma beta as a percentage rather than as a fraction. For the corona within the Sun, it will typically have a value of around β_B ~1%. For a magnetic Tokamak as proposed for a potential commercial fusion reactor it may be as high as β_B ~ 2 - 5%. For a spherical Tokamak β_B ~10 - 40%. For a Stellarator β_B ~1 - 5%. For the magnetic nozzle in an ICF engine we likely want $\beta_B < 1\%$ but tending towards unity. Otherwise, this is not an efficient use of the volume or magnetic power control.

For a space propulsion engine $\beta_B \rightarrow 1$ around the deflection point where the magnetic field pushes the charged particles. Since the plasma will then expand rearwards of the spacecraft B should decrease which means that β_B will increase. This ensures the charged particles spiral along the field lines and towards the rear of the vehicle and do not come back to the spacecraft. If the value of β_B moving away from the spacecraft does not continue to increase, then this will reduce the decoupling efficiency of the charged particles and may also decrease the jet efficiency and this is a form of plasma drag.

2.2 Larmor Radius

The gyroradius, also known as the Larmor radius, defines the circular motion of a charged particle following the path of a magnetic field. It is defined by the charged particle mass m, the perpendicular component of the velocity $v_\perp$, the proton number Z, electric charge q and the magnetic field strength B as follows:

$$r_g = \frac{mv_\perp}{ZqB} \tag{4}$$

If the plasma contacts the chamber walls this leads to significant heating. We can estimate the gyroradius for the charged particles within the plasma. According to the Daedalus study, if we assume that a D^3He fuel will give rise to the products of protons and ^4He particles and with a perpendicular velocity of 15,000 km/s then they will have a gyroradius of 0.72 cm and 1.42 cm respectively. This corresponds to a gyrofrequency of

TABLE 1: Larmor Radius of Charged Particles within Daedalus Reaction Chamber Assuming Field Strength *B* = 15.85 T and velocity = 15,000 km/s

Parameter	p^+	D	T	^3He	^4He
Z	1	1	1	2	2
Z_e	1.0072	2.0135	3.0155	3.0160	4.0026
m(kg) $\times 10^{-27}$	1.673	3.344	5.007	5.008	6.646
Q(C) $\times 10^{-19}$	1.602	1.602	1.602	3.204	3.204
r_g (cm)	0.988	1.975	2.958	1.479	1.963
ω_g (rad/s) $\times 10^8$	15.181	7.594	5.071	10.139	7.64
$r_g \times$ SM (cm)	1.976	3.95	5.916	2.958	3.926

1.52×10^9 rad/s and 7.64×10^8 rad/s respectively. These values are attained if one assumes a field strength of around ~15.85 T. Allowing for a factor of two safety margin (SM), this suggests that the gyroradius is permissible that does not get within ~3 cm of the internal reaction chamber structure. This result is consistent with the calculations of other authors [7].

However, as discussed later, we calculate that for the Daedalus the peak magnetic field strength would be around 15.85 T. The results of calculating this are shown in Table 1 along with the gyrofrequency of oscillation within the field. The calculated Larmor radius for the different charged particles is the minimum distance that must be maintained between the expanding plasma, and the reaction chamber walls if direct interaction is to be avoided. The different values of Larmor radius for the main charged particles are shown in Fig. 4 as a function of magnetic field strength.

In this study we did not get into the details of designing the magnetic nozzle for Pegasus, yet we mention the above physics issues as being critical to its operation. Others are encouraged to facilitate numerical modelling of a magnetic thrust structure along these lines such as by using Particle-In-Cell codes [8, 9]. A particular area that needs more work is the sizing of the reaction chamber volume to the plasma expansion radius since the two are likely design dependent, i.e. a larger plasma expansion would correspond to a larger reaction chamber size and where the magnetic field strength provided by the external superconductors is inversely proportional to the reaction chamber radius. The current size of the Pegasus reaction chambers was largely determined by pellet injection velocity [10].

Research into magnetic nozzles is an active field of research by others [11]. Cassibry et al [12] has been looking at the use of a novel field coil winding method, longitudinally rather than azimuthally, as a means for helping to promote a higher component of the J × B force. They have found that magnetic nozzles do appear capable of redirecting thrust from a plasma and that the coil shape which creates a largely azimuthal magnetic field are likely to lead to efficient designs. This research has continued in further experiments by Schilling *et al* [13] to include a subscale demonstration of an axial pulsed magnetic nozzle system.

2.3 Plasma Expansion

Another novel method adopted for the Daedalus spacecraft design was to employ a highly optimised hemispherical structurally conducting thin-shell wall configuration around the reaction chamber which could also act as a form of shock absorber. When the detonation of an ICF pellet occurs, the plasma will expand into the target chamber rapidly. Since the expanding plasma compresses an existing weak magnetic field into the shell this causes its field strength to be raised from sub-Tesla to 10s-Tesla within microseconds time duration. The design of the wall geometry as it goes into tension, would cause it to rebound and then push back on the plasma. This sets up a situation of steady

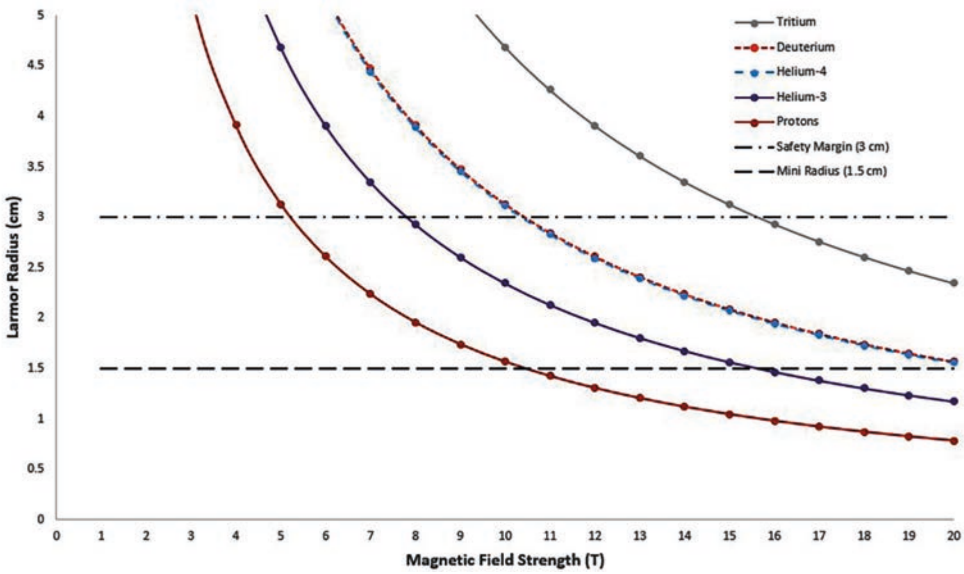

Fig.4 Estimates for Larmor Radius with Magnetic Field Strength for Charged Particles Gyrating in Field Lines.

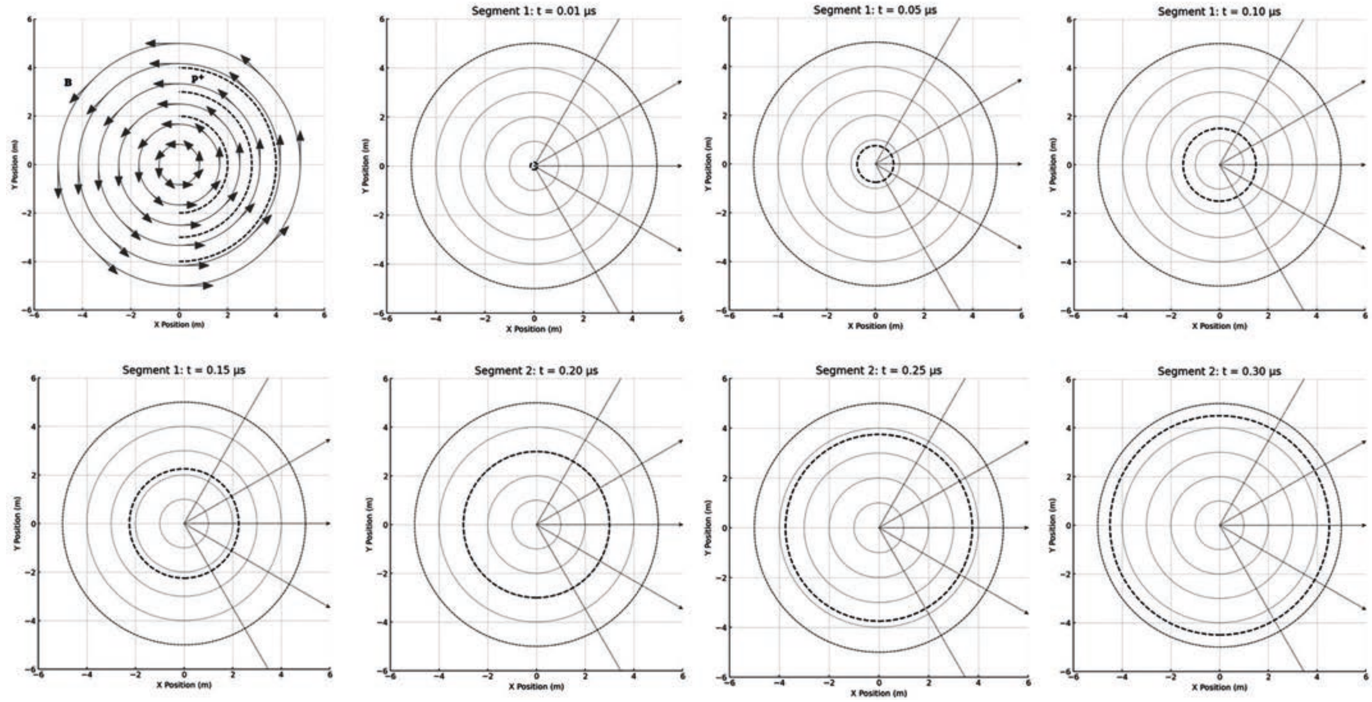

Fig.5 Thermal Expansion of Plasma Shell in Reaction Chamber.

state oscillation commensurate with the pulse detonation frequency but may lead to excessive heat loads and material fatigue.

The expansion of a single pellet detonation wave is shown in the simulation of Fig. 5 where the plasma takes of order ~0.3μs to get to the outer extent of a 5 m radius reaction chamber. Since $\beta_B \propto 1/B^2$ the stronger the field strength the lower the value of the plasma beta. However, the plasma beta is also a function of the particle density and temperature and so in principle within the engine nozzle should be very high which implies a high degree of magnetic confinement of the plasma.

In the Project Daedalus study, the authors derived a minimum condition for the magnetic field pressure as a function of the ion charge number Z, ion mass m, electron charge e, plasma expansion velocity $\bar{v}$ and distance from the plasma to the engine chamber wall R_w. The condition ensures that the Larmor radius of the ions is smaller than the nozzle radius and so effectively enabling the magnetic confinement and directionality of the exhaust products within the engine nozzle. It is given by:

$$B_o \geq \frac{3m\bar{v}}{ZeR_w} \geq \frac{1}{R_w} \tag{5}$$

Table 2 gives the values for the different parameters calculated by the Daedalus team for the first and second engine stage at R_w = 50 m, and R_w = 20 m respectively. For Daedalus they firstly calculated an approximation for B_o of 0.02 T and 0.05 T, but we have calculated it more accurately. They would then multiply this by a safety factor (SF) of around 1.5 which we have also done for the more exact calculation, and this is B_o'. This has then been rounded up to the more suitable value chosen by the Daedalus team in the definition of B_o''. We have performed a similar calculation for the 10 m and 5 m reaction chamber designs for the Pegasus, and these are also shown in Table 2. Also shown in Table 2 is the estimated number density, which is given by as a function of the chamber volume V and number of particles N in relation to the atomic numbers of the particle species (A_1+A_2) as well as the fuel capsule mass m_{cap} and Avogadro's number N_A as follows:

$$n = \frac{N}{V} = \frac{3m_{cap}N_A}{4\pi(A_1+A_2)R^3} \tag{6}$$

In the calculations for the temperature this was found to be $T = 6.992 \times 10^8$ K based on an assumed 60 keV or 9.654×10^{-15}J. We assumed $\bar{v}$ = 15,000 km/s. For the particle species we assumed protons and Helium-4 with charge number Z_1 =

TABLE 2: Calculations for Minimum Magnetic Field Strength

Parameter	Daedalus 1st	Daedalus 2nd	Pegasus (i)	Pegasus (ii)
R(m)	50	20	10	5
B_o(T)	0.0155	0.0388	0.0775	0.1551
SF	1.5	1.5	1.5	1.5
B_o'(T)	0.0233	0.0582	0.1163	0.2327
B_o''(T)	0.0333	0.0667	0.1550	0.3102
n(m^{-3})	1.0961×10^{17}	1.7127×10^{18}	1.3702×10^{19}	1.0961×10^{20}
P_B (N/m^2)	9.9961×10^7	9.9961×10^7	9.9961×10^7	9.9961×10^7
P_P (N/m^2)	1.0582×10^3	1.6535×10^4	1.3228×10^5	1.0582×10^6
β_B (%)	0.00106	0.0165	0.1323	1.0586

1.00727 and Z_2 = 4.0026, and atomic numbers A_1 =1. 00727 and A_2 = 2.01454. We note that in all cases the estimated plasma beta is very low as required, where the magnetic pressure dominates strongly over the plasma pressure near the reflection point in the magnetic nozzle. This confirms the magnetic confinement and directionality are effective without significant plasma pressure disrupting the nozzle's field structure. However, comparing the values for the plasma beta of the Pegasus reaction chambers compared to Daedalus they are not as dominant. This is particularly the case in the 5 m reaction chamber where we have β_B = 0.01059. This still indicates a dominant magnetic pressure but would be something to keep an eye on, since the point where $P_P \rightarrow P_B$ this would become an unstable magnetic nozzle configuration to be avoided. This is more likely to occur in smaller reaction chambers since the plasma pressure increases as $P_P \propto 1/R$. In a smaller chamber the plasma pressure increases dramatically whilst the magnetic pressure remains constant if the field strength is unchanged, leading to a higher β_B.

The fuel for the system was to be D^3He and was ignited at a temperature of 60 keV. The initial number density of the 50:50 fuel mixture was 0.089 g/cm^3 so that the nominal number density would be n = $N_A\rho$/A, where the Avogadro number N_A = 6.022 × 10^{23} mol^{-1}, and the average atomic mass A = (2.01410 + 3.01603)/2 = 2.515 so that n = 2.13104 × 10^{28} m^{-3}. In the Daedalus the first and second stage fuels were to be compressed by a factor of 1,000 and 2,000 respectively. This implies a compressed density for the two stages of n_1 = 2.131 × 10^{31} m^{-3} and n = 4.262 × 10^{31} m^{-3} and so a plasma pressure of 2.048 × 10^{17} Jm^{-3} and 4.097 × 10^{17} J/m^3.

Then for the plasma beta $\beta_B \rightarrow 1$, we can estimate the magnetic field strength required from the magnetic pressure. This would require an instantaneous magnetic field strength of >> 10s T for both the first and second stage respectively and assumes significant compression of the magnetic field against the field adjacent to the reaction chamber wall. To gauge the plausibility of this would require more detailed calculations than presented here. An independent analysis of the Daedalus reaction chamber and associated plasma expansion was given by others [7] where it was found that the peak pressure at the chamber wall would be around 100 MPa and that the plasma was found to expand almost spherically up to turnaround. If we equate this to a magnetic pressure that would imply a peak magnetic field strength of 15.85 T and this is the reason we have adopted this value in the earlier calculations. This is consistent with the "10s-Tesla" claim by Daedalus but also far too low to be consistent with a unity value for the plasma beta.

We also note that for Pegasus the shape of the engine reaction chamber is no longer hemispherical but more of a spheroid. This is to facilitate the arrangement of many laser beamlines positioned symmetrically around the target as it is injected into the target chamber. This helps to prevent the scenario of an asymmetric implosion symmetry of the fuel which would result in an inefficient implosion engine. The lasers will produce enormous amounts of heat and so that is the reason for the primary positioned radiators along the length of the vehicle. The engines will also produce excess heat and so that is the reason for the rear radiator fins.

2.4 Charged Particle Jet Collimation

To help visualise the motion of the charged particles being emitted from the magnetic nozzle we used a small Monte Carlo program written in Python to simulate charged particles (ions and protons) moving through a magnetic field. These originate from an expanding plasma shell, the location from which the charged particles are launched, and interact with the magnetic field via the Lorentz force where the stronger the magnetic field the tighter the spiral gyroradius.

$$F = q(E + v \times B) \tag{7}$$

But for simplicity and ease of computation we assume E = 0 so that:

$$F = q(v \times B) \tag{8}$$

They then follow the magnetic field lines and spiral around them based on a defined pitch angle. After this they exit the magnetic nozzle as the basis for the vehicle thrust. Since this is a Monte Carlo simulation the charged particles take on randomized positions and velocities as they are emitted from the shell surface. We assume a collisionless model for simplicity. The initial proton positions are randomly distributed on a ring of radius r_o = 1 m centred on the z-axis so that $x = r_o \cos\theta$, y = $r_o \sin\theta$, z = 0. This creates a hollow circular shell of plasma expansion around the pellet centre to simulate an isotropic detonation centred inside the reaction chamber.

In the simulation, to keep it simple we consider the scenario of a D^3He fuel that produces only protons and ^4He ions. We assume a simple axial field model and due to computational limits, we restrict the number of particles to a total of 500, which means 250 protons and 250 ^4He ions. The total energy that is shared between the particles is 18.4 MeV, for which the protons are 14.7 MeV or 1.602 × 10^{-13} J for a 1.67 × 10^{-27} kg proton. Each proton will start with a kinetic energy given by:

$$E = \frac{1}{2} m v^2 \tag{9}$$

So that the speed is found to be:

$$v = \sqrt{\frac{2E}{m}} \tag{10}$$

The simulation runs for a total of 100 time steps or around 20 ns. We assume an axial magnetic field strength of B_o = 15.85 T. The plasma ring is assumed to emerge to a distance 1 m from the reaction chamber surface, sufficient to allow visualisation of the particle motions and forward momentum.

By around 20 ns the charged protons, because of the pitch angle (nonzero velocity in the z-direction), steadily drift forward past Z = 1 m distance and the jet forms by Z = 2-3 m. Some of the charged particles undergo lateral dispersion since the initial velocity vectors vary randomly, which leads to azimuthal spreading and radial dispersion as they spiral outwards. They are confined transversely by the initial magnetic field but as they move away from the magnetic field there is no force to collimate them into a tighter exhaust beam, and this is why they diverge into a broader spread.

To confine the particles within a magnetic field longer this requires the use of a magnetic nozzle, such as in the user of a diverging solenoid. To simulate this, we model a diverging magnetic field near the end of the reaction chamber that redirects the spiralling particles into a narrower, axial jet. This causes any charged particles to converge in a forward direction even if they are spread out in position and helps to visualise the collimation effect even if under a very short timescale. The magnetic field shape is stronger near the origin and weaker and diverging near the rear and is given using an adjustable parameter constant $a = 2.5$, where:

$$B_z(z) = \frac{1}{(1+a(z-z_o))^2} \tag{11}$$

Since the magnetic field is only in the axial direction (B - B_z(z)), then the cross product gives the accelerations:

$$a_z = \frac{F_x}{m} = \frac{q}{m} v_y B_z(z) \tag{12}$$

$$a_y = \frac{F_y}{m} = \frac{q}{m} v_x B_z(z) \tag{13}$$

But where the Z-acceleration is zero ($a_z = 0$) since there is no electric field or magnetic gradient force in z in our simple toy model. We also apply a magnetic mirror force to push the charged particles towards the regions of stronger magnetic field strength which aids in the reflection and collimation along the axial alignment, and this is given by:

$$F_z = -\mu \nabla B = -\mu \frac{dB}{dz} \tag{14}$$

Where we apply conservation of magnetic moment so that as B(z) increases, $v_\perp^2$ must decrease and so v_z^2 must increase to conserve the total energy:

$$\mu = \frac{m v_\perp^2}{2B} \tag{15}$$

In this equation μ is conserved and where $v_\perp$ is the velocity perpendicular to the magnetic field, B(z) is the magnetic field strength along the nozzle axis. As particles move into a region of stronger B(z), to conserve μ, $v_\perp^2$ or B(z) and so $v_\perp$ will increase and the spiral tightens and rotates faster. This mirror force is added to the z-direction so that the equation becomes:

$$a_z = -\frac{1}{m} \mu \frac{dB}{dz} \tag{16}$$

However, when B(z) is very small near $z = 0$ we get a large $v_\perp$ causing the particles in the simulation to collapse radially too early. For this reason, we clamp the magnetic field to a minimum value of $B = 0.01$ T to preserve the focussing behaviour and prevent the plasma becoming unstable and therefore uncollimated. The magnetic moment is also capped to prevent unphysical mirror forces where particles could otherwise become infinite.

A strong axial magnetic field peak is applied around $Z = 1$ m to simulate the presence of a focussing solenoid coil at $\sigma = 0.2$ m to represent the width of the throat, which provides for a tighter confinement in the xy plane. This leads to a more coherent axial jet formation to be visible in the short simulation. The axial magnetic field that peaks near z_o resembles a Gaussian coil throat configuration, where the variation in B_z causes the cyclotron frequency to change, tightening the spirals and aligning particle trajectories, and is given by:

$$B_z(z) = B_o exp\left(-\frac{(z-z_o)^2}{2\sigma^2}\right) \tag{17}$$

The Cyclotron frequency is given by:

$$\omega_c = \frac{qB}{m} \tag{18}$$

So that as B increases toward the nozzle throat, the cyclotron frequency also increases, and the particles will spiral faster around the field lines. Essentially the magnetic field ramps up near the throat and so the protons will spiral and become tighter and faster. At each time step Δt we update the velocities and positions using the following equations:

$$v_x^{(t+1)} = v_z^{(t)} + a_x \Delta t \tag{19}$$

$$v_y^{(t+1)} = v_y^{(t)} + a_y \Delta t \tag{20}$$

$$x^{(t+1)} = x^{(t)} + v_x^{(t+1)} \Delta t \tag{21}$$

$$y^{(t+1)} = y^{(t)} + v_y^{(t+1)} \Delta t \tag{22}$$

$$z^{(t+1)} = x^{(t)} + v_z^{(t+1)} \Delta t \tag{23}$$

Fig. 6 shows the results of the simulation for a single engine nozzle where we see a ring of charged particles spiralling outwards into a collimated jet. For this simulation, the only par-

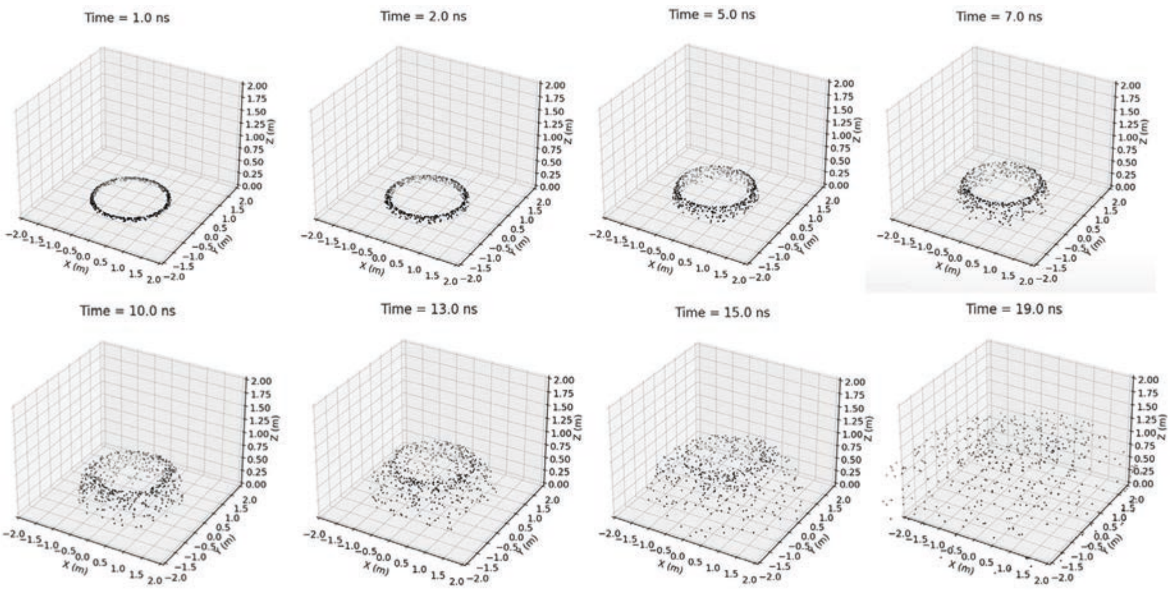

Fig.6 Thermal Expansion of Charged Particles in Magnetic Nozzle.

ticles present are protons. At the entry to the simulation the particles spiral slow and wide within a weaker magnetic field. We note that the particles spiral faster towards the throat of the simulation due to the consequence of magnetic moment conservation in a spatially varying magnetic field, which at this point is strong and so the spirals are tight and fast. The charged particles are constrained to follow the magnetic field lines whilst spiralling around them, where their motion is governed by the conservation laws. As they exit the simulation this is with decreasing magnetic field and so the spirals widen again.

Fig. 7 shows the physical properties of the proton as it transmits through a magnetic nozzle. The top charts shows that the perpendicular velocity increases as the particle enters a strong magnetic field B(z) confirming a tightening spiral. The middle chart shows how the cyclotron frequency ωc rises in the presence of the magnetic field B(z) showing that the particle is spiralling faster than expected in the absence of a magnetic field. The lower chart shows the magnetic moment μ stays approximately constant and confirms the adiabatic invariance.

We next move to a more advanced simulation in Fig. 8 where instead of one ring and a single population of particles, we move to four rings and two populations of particles which is a better approximation to the Pegasus engine configuration. The four rings simulate the Pegasus parallel thrust arrangement although for this simulation we model only 1 m rings for ease of computational capacity. As with the earlier simulation, the motion of the particles is under the Lorentz force, magnetic field and mirror force. Again, we assume a magnetic field strength of 15.85 T. Since the simulation is Monte Carlo, there is a random variation in the azimuthal angle (0-360^0) and initial position. Again, there are no particle interactions, and the protons also do not collide with each other or any other background plasma.

The maximum pitch angle was limited to θp = 10^0 and we

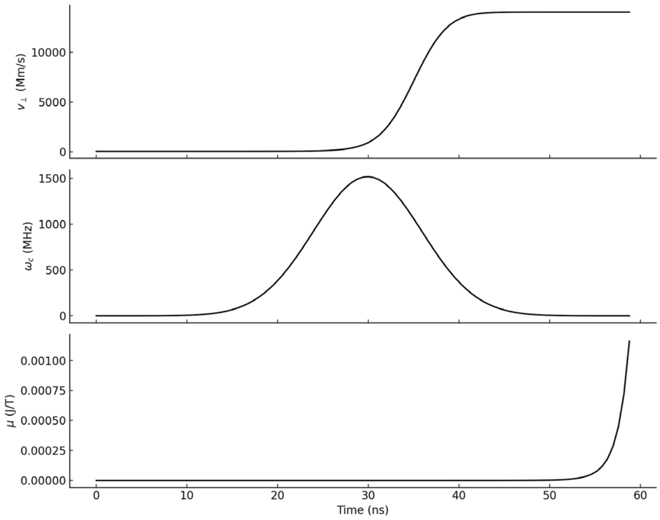

Fig.7 Physical Properties of Protons in Simulation Through Magnetic Nozzle.

also limited the positional jitter to ± 10 cm. The pitch angle is given in reference to a total speed v as the sum of the axial component speed along the B-field v_z and the transverse component perpendicular to the B-field $v_\perp$ so that:

$$\theta_p = arctan\left(\frac{v_\perp}{v_z}\right) \tag{24}$$

Where $v_\perp = vsin\theta_p$ and $v_z = vcos\theta_p$. Alternatively, the pitch angle is given by:

$$\theta_p = arctan\left(\frac{\sqrt{v_x^2+v_y^2}}{v_z}\right) \tag{25}$$

In this way the pitch angle is randomly chosen to simulate

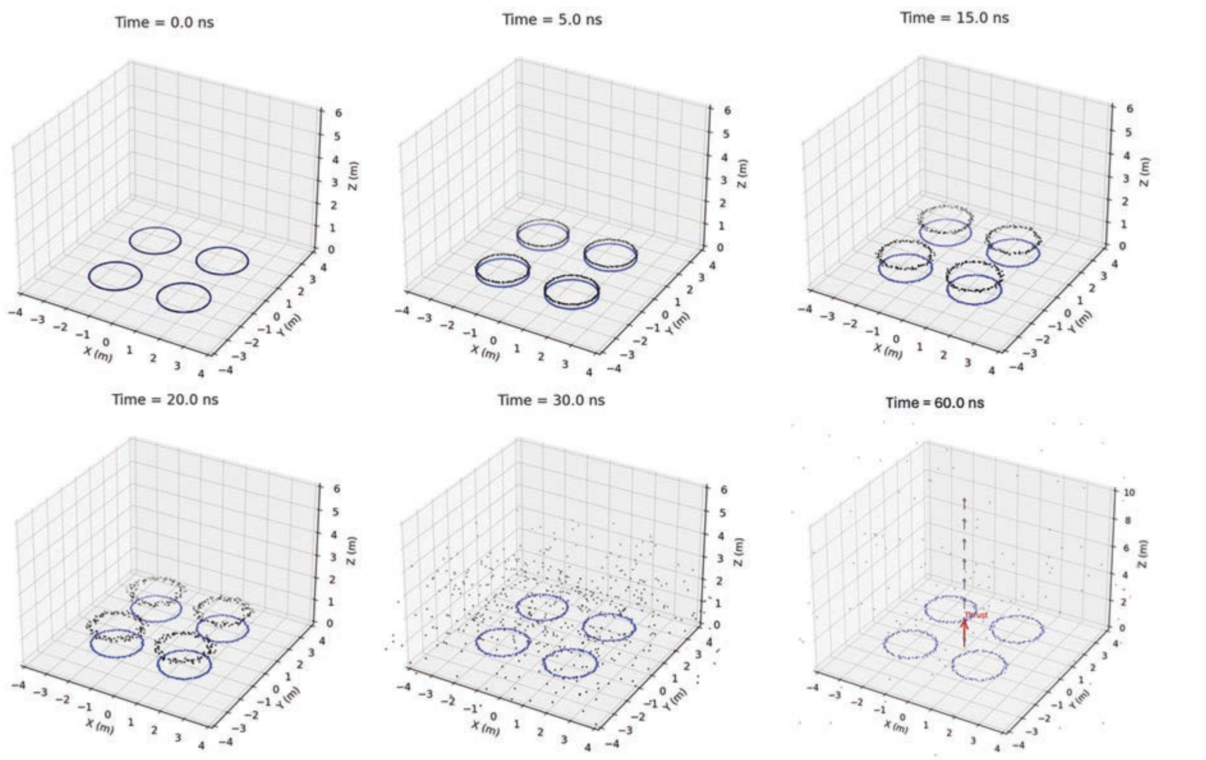

Fig.8 Thermal Expansion of Charged Particles in Four Magnetic Nozzles to Simulate the Pegasus Parallel Thrust Configuration.

a slight spread but does not go above the maximum value to limit the divergence and ensure collimation of the beam in the nozzle. The lower the value of θ_p the more collimated the jet, and the higher the value of θ_p the more divergence.

For the simulation we assumed four rings with 250 particles per ring so a total of 1,000. The rings were spaced by 3 m and each ring had a radius of 1 m. The protons have an initial kinetic energy of 14.7 MeV which is an initial speed of 5.29×10^7 m/s. The magnetic field minimum is capped to 0.01 T and peaks at 15.85 T. The mirror shape is Gaussian as earlier. The simulation is run for 60 ns with a time step of 1 ns or 30 ms/frame.

An examination of the results from the simulation shows that the ^{4}He start with a much lower velocity due to their lower kinetic energy, and so they transport outwards more slowly. With the larger mass and double the charge, the radius doesn't scale linearly, thus they tend to exhibit a smaller Larmor radius resulting in a tighter spiral confinement. In the presence of the magnetic field, due to their larger mass, they respond more slowly. The ^{4}He particles have a gyro radius one quarter that of the proton, where for the proton it is of order a few cm in size. They also have a speed of 1.3×10^6 m/s compared to 5.3×10^6 m/s for the protons, so they are four times slower in terms of transverse velocity. Therefore, for a given duration of time the ^{4}He ions can be expected to travel four times less distance.

Thus, in the simulation it looks like the ^{4}He particles remain more focussed and less dispersed compared to the protons. The simulation shows the results up to 30 ns from original start. The protons become highly dispersed by around ~30-40 ns but for the ^{4}He they become dispersed by around ~90-120 ns. It is fully acknowledged that these Monte Carlo simulations make assumptions such as no E-fields, no gradient in B, no space-charge, no collisions, and use few particles. A real ICF plasma may also be strongly non-uniform, multispecies, non-Maxwellian, subject to ExB drifts and inductive fields.

Fig. 9 shows the projected (qualitative visualization only) charged particle path trajectories for the ^{4}He (blue) and protons (black) assuming a plasma temperature of 10 keV or 100 million K. We assumed 500 particles for each population. The simulation was run until around 60 ns. This reveals a jet structure along the main axis and with a net direction consistent with the required impulse direction to generate thrust. The protons demonstrate significant radial spreading due to their thermal motion and this manifests as wider spirals and a larger divergence. Whilst the helium-4 particles remain mostly collimated on tighter paths but begin to diverge radially later.

Although this is not a full simulation of the Pegasus engine reaction chamber and magnetic nozzle it does illustrate the sort of collimated jet behaviour we might expect. Fig. 9 shows a large divergence of the jet collimation angle which should be avoided if the jet efficiency is to be minimised.

An interesting point to note is that any external observer watching the Pegasus from afar would first detect photons from Bremsstrahlung ultra-violet and x-ray emission, but then they would detect electrons, followed by protons and then other high mass ions. This might be a useful way of thinking about the search for propulsion systems from extraterrestrial civilizations in terms of the particle distributions, types and differences in times of arrival [14].

In the Daedalus reports the authors attempted to describe the placement of the magnetic field coils around the reaction chamber. They had calculated the magnetic flux shaping that would be involved in the plasma confinement and the collimation of the jet through the magnetic nozzle. They indicated the likely location of the boundary where the plasma was confined and where the exhaust flow begins. As was shown the field coils generated strong localized magnetic fields around the reaction chamber and nozzle exit, combining to produce the nominal 15.85 T near the reflection point to ensure a tight ion gyro radius and effective jet collimation through using a low plasma beta condition.

3 PROPULSION ENGINEERING

3.1 Reaction Chamber

For Project Icarus and the Pegasus design we did not go into detail on the design of the reaction chamber, and readers are referred to the Daedalus design for an example of how it might operate. For the Daedalus at 250 Hz, the first stage will accelerate for 2.05 years and the second stage for 1.76 years, which implies a total of 16.16 billion and 13.87 billion cycles for these two engines respectively. For the Pegasus with its total acceleration and deceleration time equal to 4.76 years this will involve between 150.11 billion (1,000 Hz) to 375.27 billion (2,500 Hz) cycles during the thrust phases. This is sure to lead to significant structural fatigue and so would require detailed modelling. Within Project Icarus some work has been conducted into the design of reaction chambers. This has included extensive

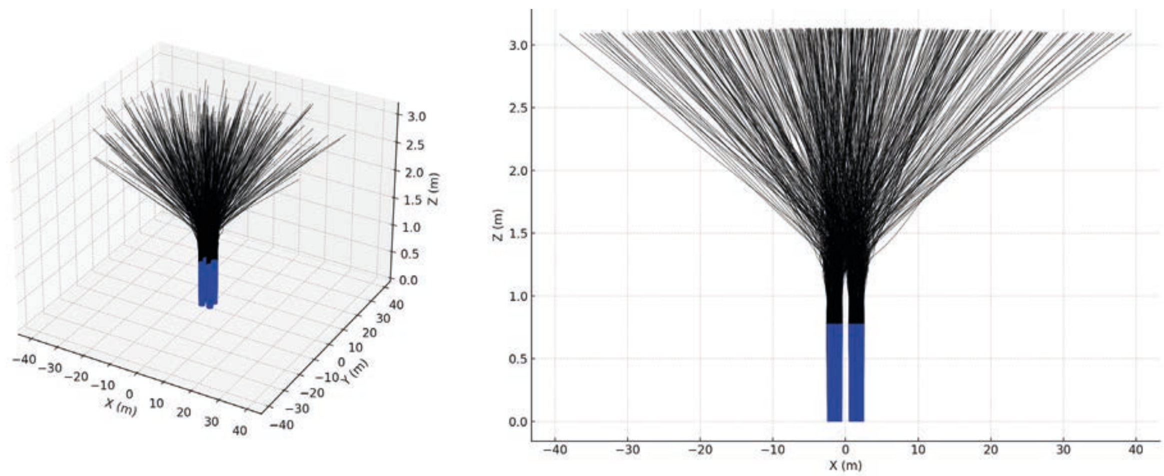

Fig.9 Jet Collimation Effect of Charged Particles in a Single Magnetic Nozzle Exhaust.

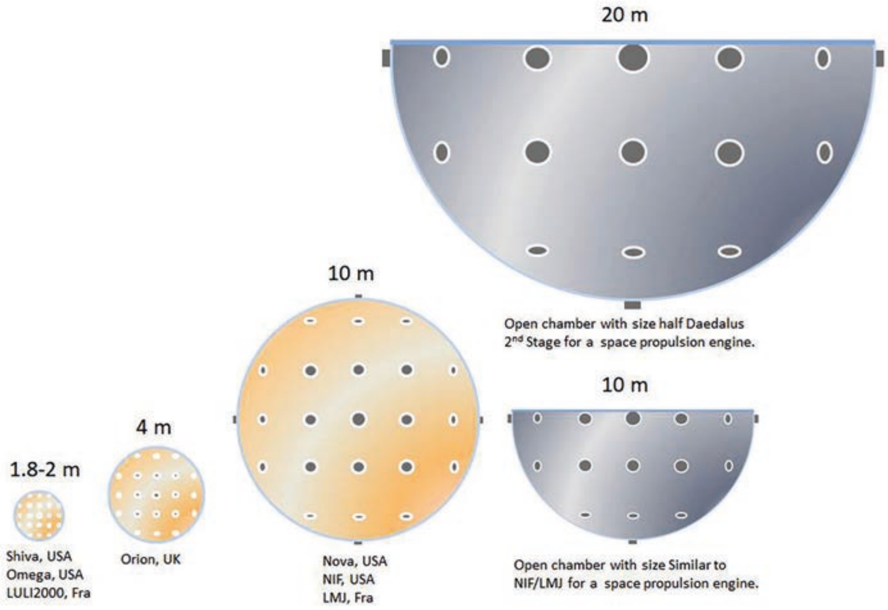

Fig.10 Types of Inertial Confinement Reaction Chambers.

finite element modelling of the thrust structure, in terms of static loading from pellet detonations and vibrational characteristics [17].

Fig. 10 shows a comparison of reaction chamber sizes typically used in inertial fusion experiments and the sizes proposed for the use of space propulsion applications. Note that whilst the experiments are closed chambers the propulsion ones are open and form hemispheres. This is necessary since the plasma exhaust will be magnetically directed rearwards for thrust generation.

The Pegasus vehicle has four engines and so operates in parallel thrust mode based on a scaled down Daedalus second stage design. In earlier work for the Pegasus *Mk1* design we had assumed that each engine has a minimum mass of 300 tonnes, which means the total engine mass is 1,200 tonnes. This was because the minimum mass for a fusion propelled ICF propulsion system is an unknown and difficult to extrapolate given the likely advances in technology that will occur in the future. The value of 300 tonnes like that derived by other authors [18, 19, 20].

However, once the design work got to the point of doing the power cycle calculations and then thermal management, it was necessary to reduce the mass of systems to achieve the one century mission requirement. For this reason, each engine in the Pegasus was specified to be of order ~100 tonnes in mass as a requirement, bringing the total to 400 tonnes, where this mass includes the reaction chamber, magnetic field coils and any ancillary parts. That said, whereas the reaction chamber radius for Daedalus was 20-40 m, for Pegasus we are looking at 5-10 m, and so the reduction in mass should also be expected. In the text below we will estimate the actual likely mass for the reaction chamber and then for the magnetic field coils in the Pegasus *Mk2* design.

We will consider two types of geometries. The first is a hemispherical reaction chamber as used in the Daedalus design. The second is an oblate spheroid design which might be more typical of what would be adopted in the Pegasus design. We start from an assumed ~300 tonnes reaction chamber mass like the Daedalus second stage with its 20 m radius chamber, and then we estimate the mass for two smaller sizes at a radius of 10 m and 5 m respectively. Since this is a case study, we examine the cases on the assumption of molybdenum material with a density of ρ = 10,280 kg/m^3. For a hemispherical reaction chamber the volume and mass of a hemispherical shell (half-sphere) is given by:

$$V = \frac{2\pi}{3}\left(R_{outer}^3 - R_{inner}^3\right) = \frac{2\pi}{3}\left(R_{outer}^3 - (R_{outer} - \delta x)^3\right) \quad (26)$$

$$m = \rho V = \frac{2\rho\pi}{3}\left(R_{outer}^3 - (R_{outer} - \delta x)^3\right) \quad (27)$$

On the assumed density and 20 m outer radius, running through the different values suggests a shell thickness of order δx = 1.18 cm, but for a slightly higher mass of 304.5 tonnes. We can then use this assumed structural thickness to estimate the mass for the smaller designs, at one half and one quarter scale, consistent with a large, medium and small oblate spheroid. As shown in Table 3 this leads to a mass of 76.1 tonnes for a 10 m reaction chamber and 19 tonnes for a 5 m reaction chamber. Similarly, we can examine the case of the same reaction chamber radii, but for a different geometry. We consider an oblate spheroid. The results are also shown in Table 3, and this suggests a mass of 37.5 tonnes and 4.6 tonnes for the 10 m and 5 m reaction chambers respectively. Although all these masses must be multiplied by four since there are four engines.

For the oblate spheroid calculations, the volume was given as a function of the equatorial (horizontal) radius *a* and a polar (vertical) radius *b* so that:

$$V = \frac{4}{3}\pi a^2 b \quad (28)$$

So that the shell volume is given by:

$$V_{shell} = V_{outer} - V_{inner} \quad (29)$$

Substituting

$$V_{shell} = \frac{4}{3}\pi a^2 b - \frac{4}{3}\pi a_i^2 b_i = \frac{4}{3}\pi\left(a^2 b - a_i^2 b_i\right) \quad (30)$$

TABLE 3: Mass of Molybdenum Reaction Chambers

Design	Shape	Radius (m)	Height (m)	Mass (tonnes)	Mass×4 (tonnes)
1	Hemisphere	20	20	304.5	1,220
2	Hemisphere	10	10	76.1	304.4
3	Hemisphere	5	5	19.0	76.0
1	Oblate Sphere	20	16	300.0	1,200
2	Oblate Sphere	10	8	37.5	150
3	Oblate Sphere	5	4	4.6	18.4

Then the mass is given by the product of the density and volume of the shell in addition to a scaling factor derived to be 300 tonnes/783 tonnes = 0.383, so that:

$$m = \rho V_{shell} \times 0.383 \quad (31)$$

For the medium reaction chamber this leads to a = 10 m, b = 8 m, a_i = 9.9882 m, b_i = 7.99528 m, implying a mass of 37.5 tonnes. For the small reaction chamber this leads to a = 5 m, b = 5 m, a_i = 4.9882 m, b_i = 3.99764 m, implying a mass of 4.6 tonnes. Therefore, for our preferred 5 m reaction chamber in Pegasus, with its four parallel thrust engines, we are looking at an estimated mass of between 18.4 tonnes (oblate spheres) to 76 tonnes (hemispherical). We allow for some design margin and factor in additional mass for reaction chamber ancillaries and so we allocate 10 tonnes mass for each reaction chamber which comes to a total of 40 tonnes for all four engines. Figs 11 and 12 show the cross sections for these different types of reaction chamber geometries.

3.2 Magnetic Field Coils

Now that we have defined the potential reaction chamber geometry for the Pegasus, we must also define the magnetic field coils. We envisage that there are four of these per engine and they wrap around the external circumference of each engine. Collectively they act to generate a peak magnetic field strength of order 15.85 T, like the Daedalus second engine stage. Since the reaction chambers are smaller and the ICF pellets are smaller, we likely would get away with a field strength less than this. But for this exercise we will assume the same field strength in attempt to estimate the mass of the field coils. The sort of set up we imagine is illustrated in Fig. 13, which shows a single field coil with its current windings, and then four field coils wrapped around a single engine.

Table 4 shows the current, radii and axial placement positioning for the magnetic field coils in the Daedalus first and second stage designs. Scaling from the second stage, we have then generated proportional values and position for the Pe-

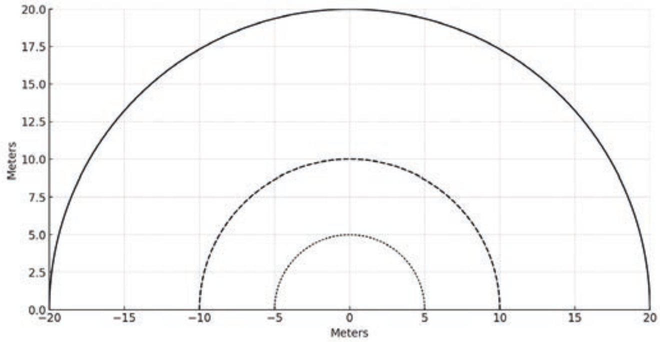

Fig.11 Cross Sections for Hemispherical Reaction Chambers.

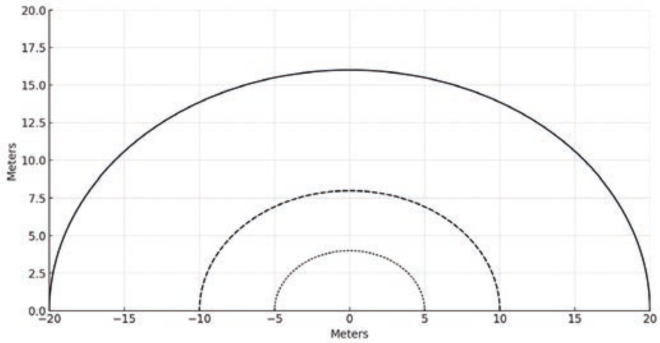

Fig.12 Cross Sections for Oblate Spheroidal Reaction Chambers.

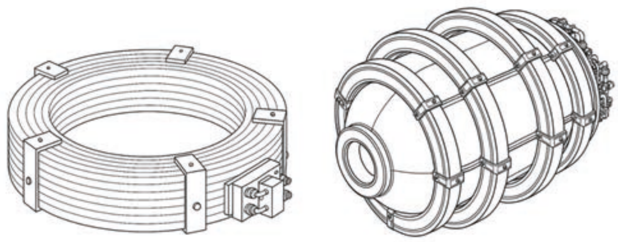

Fig.13 Illustration of Magnetic Field Coils.

TABLE 4: Assumed Magnetic Coil Positions for radius *r* and axial placement *a* where the 5-10 m chamber radius have been scaled to the Daedalus second stage, first-order engineering scaling

Parameter	Daedalus 1st	Daedalus 2nd	Pegasus (i)	Pegasus (ii)
R(m)	50	20	10	5
SF	--	1.0	0.25	0.0625
I(MA)	9.88, 1.05, 6.16, -6.83	9.0, 0.95, 5.61, -6.22	2.25, 0.238, 1.403, -1.555	0.562, 0.059, 0.351, -0.389
r(m)	12.32, 39.6, 55.0, 55.0	5.6, 18.0, 25.0, 25.0	2.8, 9.0, 12.5, 12.5	1.4, 4.5, 6.25, 6.25
a(m)	0.0, 17.6, 44.0, 55.0	0.0, 8.0, 20.0, 25.0	0.0, 4.0, 10.0, 12.5	0.0, 2.0, 5.0, 6.25

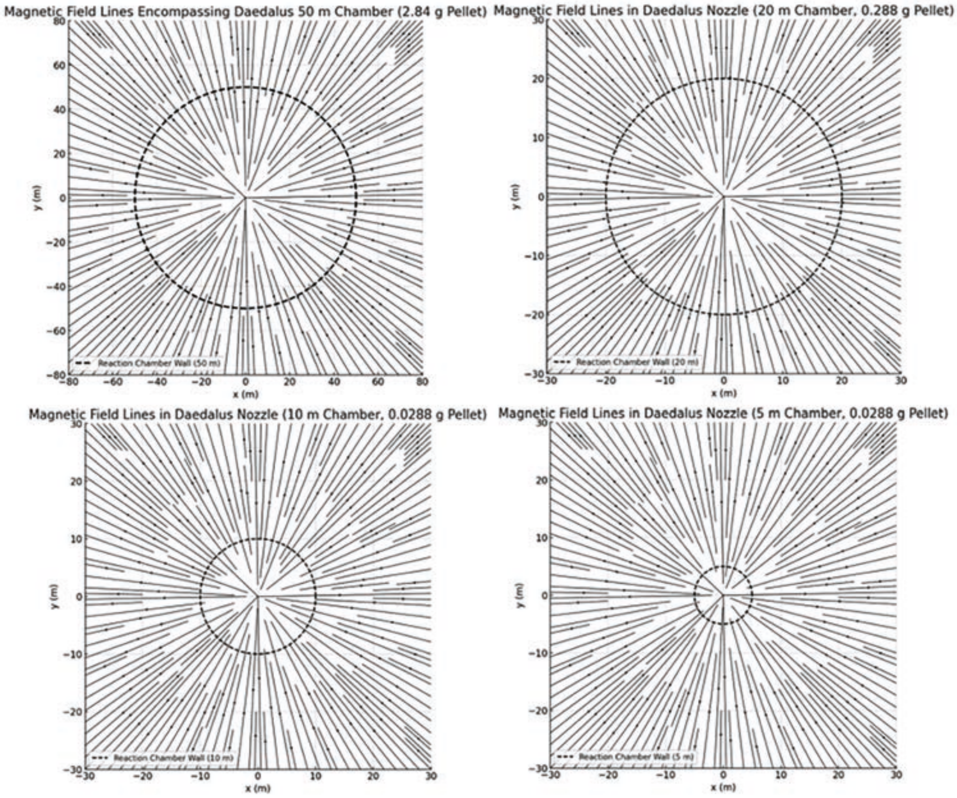

Fig.14 Magnetic Field Geometry in Thrust Direction for Charged Particle Emission from Engine Nozzle of Different Reaction Chamber.

gasus on the assumption of a 10 m and 5 m radius reaction chamber. The scaling was based on the radius relative to the Daedalus second stage, so that if the radius dropped by half, then the current was scaled down by $0.5^2 = 0.25$, and if the radius dropped by one quarter, then the current was scaled down by $(0.25)^2 = 0.0625$. The Pegasus design values are also shown in Table 4.

The coil current magnitude drops progressively to shape the magnetic field profile, where it is strongest near the chamber throat for effective plasma reflection and collimation. As it moves away from the chamber, the weaker fields are sufficient to maintain collimation whilst also allowing for expansion and divergence. If the downstream magnetic field were too strong this would increase the magnetic drag and cause reflection of the exhaust ions and bring them back to the vehicle structure. Therefore, the goal is to have a controlled divergence downstream with the magnetic field tapering designed to match the nozzle geometry.

Note also that the final coil current is negative. This creates a local reversal or dip in the magnetic field direction to form a magnetic mirror and control the field gradient. This facilitates the plasma reflection at the nozzle reflection point, beam collimation and a reduction in the divergence of the exhaust plume. To summarise, the positive current field lines align in one direction, creating a continuous outwardly expanding field, whereas the negative current field line locally opposes the field to create a pinch or reflection region. The field lines pinch inward near the reflection points and then expand outward downstream, and this was also observed in the original Daedalus calculations.

Fig. 14 shows a simulated calculation for the likely magnetic field flux lines that originate from the centre of the reaction chamber within a magnetic nozzle. This is shown for the case of the two Daedalus sized engines at 50 m and 20 radii but also for the Pegasus sized engines at 10 m and 5 m radius.

Fig. 15 shows a simulated calculation for the likely field lines seated within the positioning of the magnetic field coils that surround the magnetic nozzle. This is also shown for the Daedalus (50 m and 20 m radius) and Pegasus (10 m and 5 m radius) designs. Fig. 16 shows a simulated calculation for the likely magnetic field lines that originate from four field coils surrounding each engine, within a four-engine parallel thrust configuration as for the Pegasus design. This is shown for the 10 m and 5 m reaction chamber cases.

In estimating the field coil properties, we can start with the assumption that the current that is achievable depends only on the coil radius and not the geometry of the reaction chamber. This means that the properties we derive will equally apply to the hemispherical or oblate spherical reaction chambers. The magnetic field strength B for a single circular coil is given by the Biot-Savart equation for the current I and radius R as follows:

$$B = \frac{\mu_o I}{2R} \quad (32)$$

Where $\mu_o = 4\pi \times 10^{-7}$ H/m. This applies to a circular loop in free space, and the magnetic field is measured at the centre of the loop, provided the coil radius and position are the same and the current and coil shape remain unchanged. If any of this change, such as due to the shape of the reaction chamber, then this may alter the magnetic field properties. A caveat to this is that with different reaction chamber geometries, internal to the chamber the field geometry will be different. For example, a hemispherical geometry may cause the magnetic field lines to diverge more near the equator, and an oblate geometry may contain more field lines tightly packed near the poles. For a

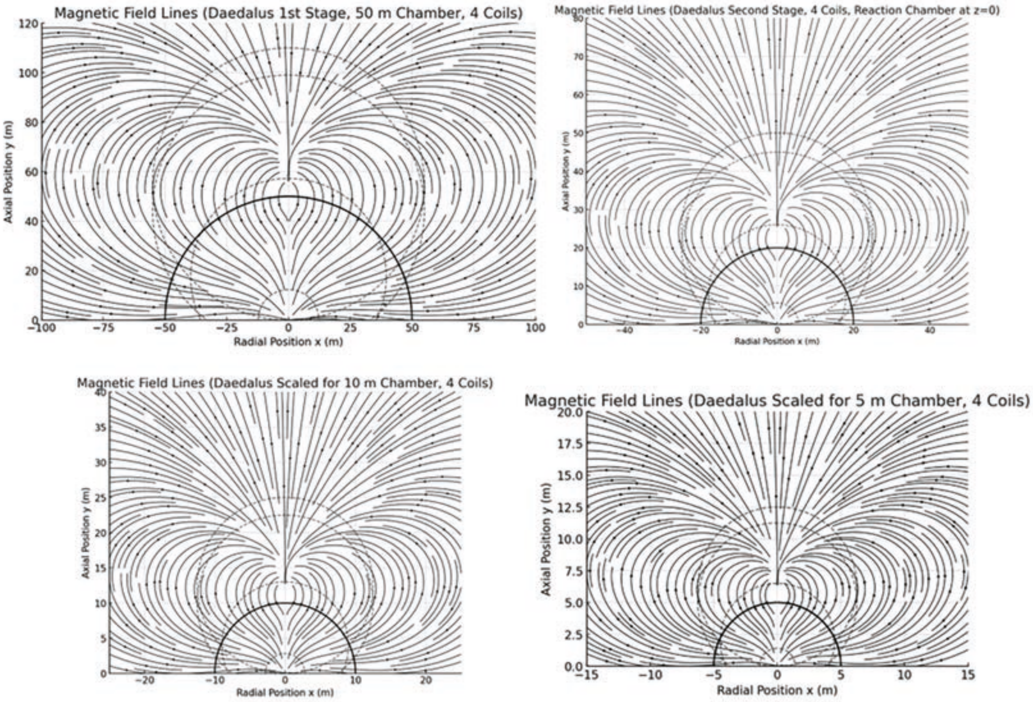

Fig.15 Magnetic Field Coil Geometries for Reaction Chamber Sizes (50 m, 20 m, 10 m, 5 m).

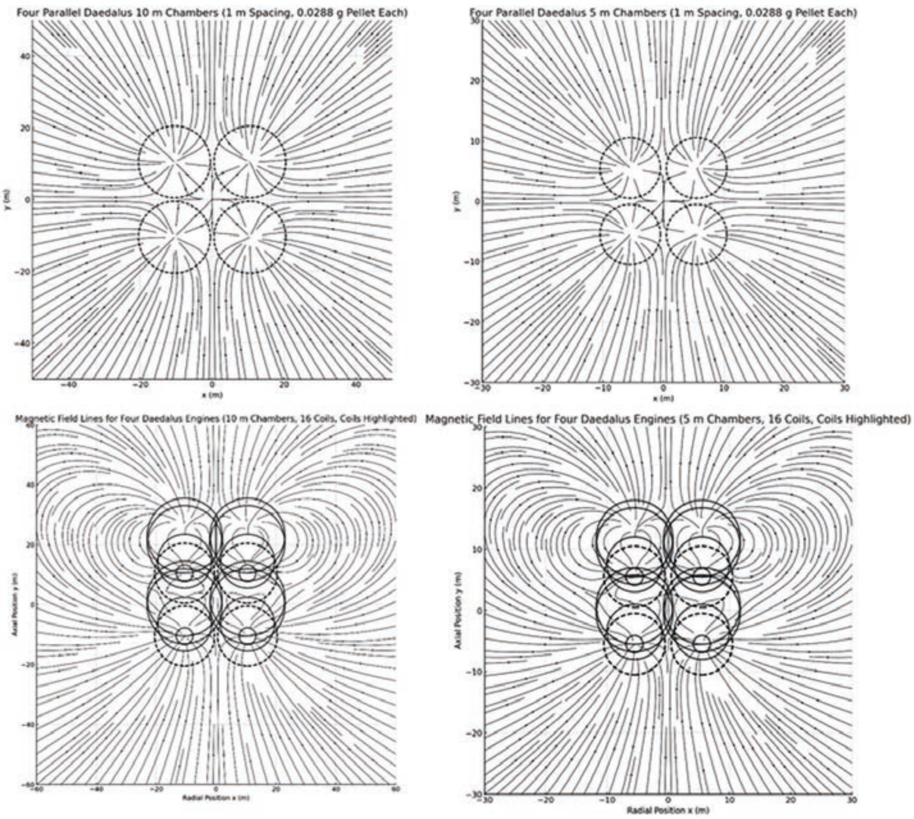

Fig.16 Four Reaction Chambers with Interacting Magnetic Field Geometries (5 m and 10 m radius).

field coil of cross-sectional area A and material density ρ the length and volume of the conductor per coil is given by:

$$L = N2\pi R \tag{33}$$

$$V = LA \tag{34}$$

Then the mass per coil is

$$m = V\rho \tag{35}$$

Since we are starting with the assumed magnetic field strength of 15.85 T, then we can re-arrange for an estimate of

TABLE 5: Estimated Properties of Magnetic Field Coils for Pegasus Engines

Design	Chamber Radius (m)	Coil Radius (m)	Current (MA) [1 turn]	Mass (tonnes)	Current (MA) [10 turns]	Mass (tonnes)	P (TW)
1	20	16	403.6	506.7	40.4	5,066.8	191,539.5
2	10	8	201.8	253.3	20.2	2,533.4	2,110.5
3	5	4	100.9	126.7	10.1	1,266.7	2,283.3

the required current as:

$$I = \frac{2RB}{\mu_o} \quad (36)$$

where we assume a coil radius $R_c = 0.8 \times R$, where R is the radius of the reaction chamber. Table 5 then shows the estimated current for the different size reaction chambers. It is fully acknowledged by the author that the specification of 100s MA turns and 1,000s TW-scale power levels are well outside of existing technology limits

Instead of a single coil design we can also examine the use of a multi-turn coil design, which reduces the current required for increased number of turns. This is given by using our earlier equation for the magnetic field strength and re-arranging it:

$$B = \frac{\mu_o NI}{2R} \quad (37)$$

So that:

$$N = \frac{2RB}{\mu_o I} \quad (38)$$

Fig. 17 shows the required current as a function of the number of coil turns to generate the required 15.85 T magnetic field. This is shown for the different reaction chamber sizes. We note that the required current drops rapidly as you increase the number of turns in a multi-turn system. The larger the reaction chamber, the higher the current per turn needed for the same number of turns. Note that this is a Logarithmic scale plot, which emphasizes the impracticality of low turn coils for large radius systems.

Note that whilst increasing the number of turns in a coil reduces the current per turn, it also comes with some engineering disadvantages. The more turns there are the longer the wire length which means that the total system mass increases. The inductance will also increase in proportional to the number of turns squared, which is bad for nuclear pulse engines since it slows down the response time and limits the rate of change in the magnetic field. The superconducting wires must also be kept below a critical temperature and the larger the number of turns the more surface area there will be to cool. So ideally, we want a high number of coil windings to reduce the current requirement, but low enough to minimise inductance, coil mass and cooling requirements. For a single coil system with inductance on the loop L and current I the total energy stored is given by:

$$E = \frac{1}{2}LI^2 \quad (39)$$

Where the energy is delivered over a pulse time t_d so that:

$$P = \frac{E}{t_d} = \frac{1}{2}\frac{LI^2}{t_d} \quad (40)$$

For a multi-turn continuous coil system, the power is a function of the resistive heating loss:

$$P = I^2\mathcal{R} \quad (41)$$

Where $\mathcal{R}$ is the resistance of the total conductor and $\mathcal{R} \approx 0$ for a superconductor and so there will be no resistive losses, although power would still be required to cool the cryogenic systems. For a 5 m reaction chamber with an inductance of $I = 2.2426 \times 10^{-5}$, this leads to an energy requirement of 114.17 GJ and a pulsed power requirement of 2,283.32 TW, assuming 50 μs pulsed operation to reach 15.85 T. The power required for the other cases is also shown in Table 5. These are enormous power requirement and suggest a need for significant technological breakthroughs before such an engine becomes viable.

For the Pegasus model, and for the purpose of minimising the mass, we assume a 5 m reaction chamber radius with a single coil turn which translates to a current of 100.9 MA and a mass of 126.7 tonnes per engine. For all four engines, this would then become 403.6 MA and a mass of 506.8 tonnes. To fit within our mass budget (defined to achieve the ~ one century mission) and accepting we may not have to achieve 15.85 T but a number lower than this e.g. for 10 T in a single turn coil, using 5 m chamber the mass is of order 63.7 tonnes. For a 10 m chamber this would be 127.2 tonnes, and 254.6 tonnes in a 20 m chamber. In a fusion propulsion engine, the higher the magnetic field strength the longer the confinement time of the plasma. We also assumed they were all at the same radius when in fact two would be smaller. We allow for some technological developments and allocate 100 tonnes for the field coils per engine which includes any materials for cooling, which is 400 tonnes in total. Note that for the field coil calculations we assumed a material density of 8,400 kg/m³ which is typical for a superconducting cable.

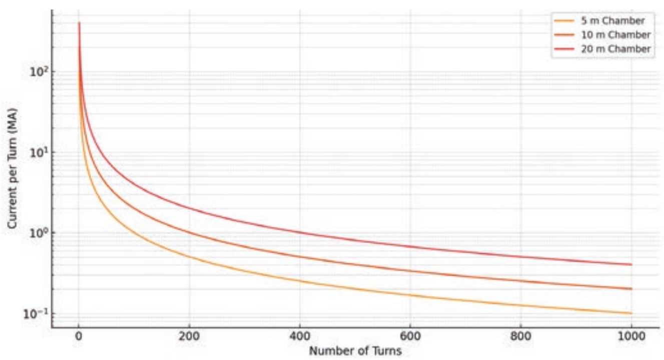

Fig.17 Required Current Per Turn vs Number of Turns for a 15.85 T Magnetic Field.

4 CONCLUSIONS

This paper has presented further details for the Pegasus spacecraft concept design rendezvous mission as a part of Project Icarus, with emphasis on the propulsion element and a discussion on some of the associated technologies and expected physics issues. This follows on from the earlier propulsion paper [6] and collectively they both describe the Pegasus *Mk2* propulsion system.

We described the value of the plasma beta particularly around the deflection point where it is the aim to guide any charged particles away from the vehicle structure. We described the Larmor radius of charged particles within the magnetic field lines of the nozzle and the requirement to maintain a safe distance from the reaction chamber walls. A description was given of the plasma expansion from the point of detonation and how this evolves to a minimum field strength. The charged particles within a collimated jet were also described, where any substantial divergence of the jet would result in a decreased jet efficiency. We discussed reaction chamber sizes and geometry as well as the use of magnetic field coils.

We acknowledge there are many technologies, particularly relevant to the propulsion system, that we have not discussed in this work, and this is because time had run out, and the project had been bought to a close. This includes systems like the induction system for which using pick-up coils would extract energy from an induced voltage as the plasma fireball expands against the externally generated magnetic field, where it would then be transmitted down to a capacitor for energy storage to fire the next laser pulse. In the power systems paper [21], we have merely specified the required power level to be inducted and not described the engineering operation of this system. Although we default to the Daedalus design for how this might operate.

Acknowledgements

The author would like to thank Rob Swinney, Robert Freeland and Michel Lamontagne for discussions in relation to the Pegasus spacecraft concept design. The author also acknowledges the assistance of artificial intelligence, Orin, in helping to calculate the magnetic field properties of reaction chambers and charged particle propagation in jet collimation. For one of the final papers of Project Icarus, this symbiotic relationship feels providential.

REFERENCES

1. K. F. Long, M. Fogg, R. Obousy, A. Tziolas, A. Mann, R. Osborne, A. Presby, "Project Icarus: Son of Daedalus – Flying Closer to Another Star", *JBIS*, **62**(1/12), 403-414, 2009.
2. K. F. Long, M. Fogg, R. Obousy, A. Tziolas, A. Presby, A. Mann, R. Osborne, "Project Icarus: Terms of Reference Document", Internal Document, 4 November 2009.
3. K. F. Long, R. K. Obousy, "Project Icarus: Project Programme Document (PPD) – Overview Project Plan Covering Period 2009 2014, Incorporating Major Task Plan for Phase III Concept Design Covering Period May 2010-April 2011", Internal Report, Published 12 May 2010.
4. A. Bond, A. Martin, "Project Daedalus: The Mission Profile", Final Study Report, *JBIS*, Special Supplement, S37-S42, 1978.
5. K. F. Long, "Project Icarus: The Pegasus Spacecraft Concept Design Engineering Systems Description", *JBIS*, **78**(6), 186-205, June 2025, DOI https://doi.org/10.59332/jbis-078-06-0186
6. K. F. Long, "Project Icarus: The Pegasus Spacecraft Concept Design ICF Propulsion for an Interstellar Rendezvous Mission – Part A", *JBIS*, **78**(12), 402-421, December 2025, DOI https://doi.org/10.59332/jbis-078-12-0402
7. J. O. Elliott & W. K. Terry, "Plasma Expansion in the Daedalus First Stage Engine", *JBIS*, **38**(3), 120-128, March 1985.
8. T. D. Arber, K. Bennett, C. Brady, "Contemporary Particle-In-Cell Approach to Laser-Plasma Modelling", *Plasma Phys. Control. Fusion*, **57**, 113001, 2015.
9. C. Brady, Epoch, *An Open Source PIC Code Developed for High Energy Density Physics*, University of Warwick, 2014.
10. K. F. Long, M. Lamontagne, "Project Icarus: Pellet Injection System for the Pegasus Spacecraft Concept Design", *JBIS*, **78**(6), 206-215, June 2025, DOI https://doi.org/10.59332/jbis-078-06-0206
11. T. Kojima, T. Morita, N. Yamamoto, "Analysis of Plasma Detachment in the Magnetic Thrust Chamber using Full Particle-in-Cell Simulation", *High Energy Density Physics*, **36**, 100814, 2020.
12. J. Cassibry, B. Winterling, K. Schillo, "Pulsed Magnetic Nozzle for Fusion Propulsion", *JBIS*, **71**(4), 119-125, April 2018.
13. N. Schilling, N. Yamamoto, T. Morita, H. Nakashima, K. Koba, J. Cassibry, "Sub-Scale Demonstration of an Axial Pulsed Magnetic Nozzle for Nuclear Propulsion Systems", *JBIS*, **77**(8), 277-283, August 2024. DOI: https://doi.org/10.59332/jbis-077-08-0277
14. K. F. Long, "A Case Study in Characterising Nuclear Propulsion Emission Signatures from Astrophysical Sources", *JBIS*, **77**(6), June 2024. DOI: https://doi.org/10.59332/jbis-077-05-0254
15. G. P. Sutton, O. Biblarz, *Rocket Propulsion Elements*, Seventh Edition, John Wiley & Sons, 2001.
16. K. F. Long, "Operational Performance Parameter Range in ICF Propulsion Theory", *Acta Astronautica*, 2010, 303-310, May 2023.
17. S. K. Reddy and H. Benaroya, "Study of Daedalus Interstellar Spacecraft Reaction Chamber and Thrust Chamber", *JBIS*, **68**(1/2), 33-43, January/February 2015.
18. D. F. Spencer, L. J. Jaffe, "Feasibility of Interstellar Travel", *Acta Astronautica*, **9**, 49-58, 1963.
19. R. Hyde, L. Wood, J. Nuckolls, "Prospects for Rocket Propulsion with Laser Induced Fusion Microexplosions", AIAA, 72-1063, Presented at the *8th Propulsion Joint Specialist Conference, 29 November-01 December 1972*.
20. C. H. Williams, L. A. Dudzinski, S. K. Borowski, A. J. Juhasz, "Realizing *2001: A Space Odyssey*: Piloted Spherical Torus Nuclear Fusion Propulsion", NASA/TM-2005-213559, AIAA-2001-3805, March 2005.
21. K. F. Long, "Project Icarus: The Pegasus Interstellar Spacecraft Propulsion Power Cycle", JBIS, 78(10), 330-343, October 2025, DOI https://doi.org/10.59332/jbis-078-10-0330

Received 30 July 2025 **Approved** 3 October 2025

Index

VOLUME 78, 2025

Contents by theme

Contents by subject

Contents by author

JBIS
Journal of the British Interplanetary Society

New Copyright Agreement

In line with most of the academic publishing world, *JBIS* is moving towards an Open Access approach to copyright and author's reproduction rights. The Journal has selected a hybrid model, which offers prospective authors two choices.

Green Open Access

This is the closest to the previous copyright agreement. Publication is free to the author. The Society retains copyright of the typeset version, which will be offered for sale on the Society's website. The author retains copyright of the manuscript version of the paper (the "Postprint"), but is embargoed from any dissemination of it for one year after the *JBIS* publication date.

Gold Open Access

This new arrangement gives the paper open access to the public on receipt of a fee from the author. Upon payment of an Article Processing Charge (APC), the author has copyright of the typeset version of the paper as it appears in *JBIS* and is free to disseminate it in any way deemed appropriate. However, the author also agrees that the paper will be available as a free download on the BIS website under a Creative Commons copyright licence (type CC-BY-NC).

Article Processing Charges

	Non-fellows	**BIS Fellows**
New papers[1]	£100	£60
Previous papers[2] <5	£20/paper	£12/paper
Previous papers[2] >5	£17/paper	£10/paper

[1]New papers are those where the paper acceptance date is after 1 January 2021

[2]Previous papers are those already published. The fee converts any prior copyright arrangement to Gold Open Access

The choice of Open Access scheme has no impact on the handling of a paper through the peer review process (referees are not informed of the author's choice), or on the priority it is given for publication. In both the Green and Gold Access options, the copyright status of the original paper (up to the corrected version following peer review) remains the same. The differences are in the copyright status of the typeset version, and in the embargo restrictions on dissemination of the original version.

JBIS
Journal of the British Interplanetary Society

VOLUME 78 NO.12 DECEMBER 2025

www.bis-space.com

ISSN 0007-084X PUBLICATION DATE: 1 DECEMBER 2025